Variability of Snow Cover in Rough Terrain

Master Thesis - Geo 511

Franziska Mohr (10-730547)

Supervision: Prof. Dr. Jan Seibert*, Dr. Tobias Jonas** and Nena Griessinger**

Responsible Faculty Member: Prof. Dr. Jan Seibert

Zürich 30. September 2015

* University of Zurich, Department of Geography, Winterthurerstrasse 190, Zürich

** WSL, Federal Institute for Snow and Avalanche Research SLF, Flüelastrasse 11, Davos Dorf (tobias.jonas@slf.ch, nena.griessinger@slf.ch)

Abstract

In the Alps a considerable part of the annual precipitation falls as snow. During winter, water is stored in the accumulating snow cover. When snow starts melting in spring it crucially influences discharge. Forecasts of melting events are essential for industries relying on water (e.g. water power plants, tourism). However, they are even more important to be able to predict heavy flood events caused by when heavy rainfalls and snowmelt coincide. The key for snowmelt predictions are accurate estimations about the amount of water stored in the snow pack as well as a correct modelling of melting patterns and rates. In recent years huge progress was made in developing such models. Yet there is still the wish to ameliorate such models with deeper knowledge of snow ablation gained from field observations or modelling approaches. In this master thesis, existing snowmelt theories were linked to high resolution SWE data collected with ground penetrating radar (GPR) during ablation season.

Currently there are numerous methods to measure snow cover. In recent years many studies were using LiDAR technology to measure height changes in snow cover and relate them to accumulation and melting events. Although providing a high spatial resolution, LiDAR measurements have the disadvantage that it does not provide direct snow water equivalent (SWE) measurements. However since SWE is the crucial parameter to describe SWE it is of interest to confirm scientific findings made with observation of HS with real time SWE measurements. A possible way to determine SWE directly is by using ground-penetrating radar (GPR). To collect such SWE data repeated field campaigns using GPR were made in the vicinity of Davos during the ablation season of winter 2014/2015.

With the assessed GPR data it was then possible to test snowmelt theories at a hill slope scale with a dataset including both HS and SWE data. In a first step the GPR data was applied to the hysteresis approach as first proposed by Egli and Jonas (2009). Results showed that the hysteresis approach is also applicable on at an hill slope scale and shows similar results when using SWE data instead of HS. Also it was investigated whether heterogeneous snowmelt is linked to the topographic parameters such as terrain roughness. Terrain roughness or other terrain parameter could not be directly linked to snow melt behaviour. However there was a differing melting rates found within the transects of the first measurement campaign (March) that was not observable for the second measurement campaign (April). It could be therefore possible that the difference in snowmelt behaviour at the two fieldsites is linked to a change of sun angle between the two measurement campaigns.

Zusammenfassung

In den Alpen fällt ein grosser Teil des jährlichen Niederschlages als Schnee. Während der Wintermonate sammelt wird in der wachsenden Schneedecke immer mehr Wasser gespeichert. Aus verschiedenen Gründen ist es wichtig zu wissen, wie viel Wasser am Ende des Winters in der Schneedecke gespeichert ist und zu welchem Zeitpunkt es zurück in den Abfluss gespiesen wird. Zum Beispiel sind solche Vorhersagen für Wasserkraftwerke wichtig. Genau so wichtig sind solche Prognosen um potentielle Überflutungen vorherzusehen, wenn z.B. starke Niederschläge mit der Schneeschmelze zusammenfallen. In den letzten Jahren wurde viel Fortschritt gemacht in Modellierungen, welche solche Vorhersagen unterstützen. Es gibt jedoch immer Punkte, welche noch nicht bis in das letzte Detail untersucht sind. Z.B. ist es bis anhin letztendlich nicht klar, ob räumliche Terrainunterschiede einen Einfluss auf das Schmelzverhalten haben oder nicht.

Heute gibt es immer genauere Methoden um solche Prozesse zu messen. Beispielsweise werden sich wiederholende LiDAR Messungen gemacht, um Veränderung der Schneehöhe während der Akkumulationsphase und der Schneeschmelze zu beobachten. Diese Art von Messungen ergeben räumlich hoch aufgelöste Resultate von der Veränderung der Schneehöhe (HS), jedoch sind sie nicht imstande Schneewasseräquivalent (SWE) direkt zu messen. Ein Weg um SWE direkt messen zu können ist der Gebrauch von einem Bodenradar (GPR). Für die Masterarbeit wurden während der Schneeschmelze im Frühjahr 2015 periodisch Feldarbeiten in der Nähe von Davos ausgeführt um HS sowie SWE mit einem GPR zu messen.

Die erhaltenen Daten wurden gebraucht um bekannte Schneeschmelztheorien auf dieser kleinen Skala zu überprüfen und mit SWE Daten zu ergänzen. Z.B. wurde ermittelt ob der Hysteresis Ansatz von Egli und Jonas (2009) einerseits auch auf dieser kleinen Skala, andererseits auch für SWE gilt. Die Resultate zeigen, dass der Hysterese Ansatz auch auf dieser kleinen Skala und bis zu einem gewissen Grad auch für SWE Daten gilt. Es wurden auch Analysen vorgenommen um zu untersuchen, ob heterogene Schmelze an den Messorten beobachtet werden kann. Für den tieferen Messort bei Monbiel, wo im März gemessen wurde, konnten unterschiedliche Schneeschmelzraten, abhängig vom Ort im Tal, beobachtet werden. Für die höhere Messstelle im Sertigtal, wo im April gemessen wurde, konnte eine solche Beobachtung nicht gemacht werden. Es konnten nur schwache Korrelationen mit Terrainparameter beobachtet werden. Es wird deshalb vermutet, dass früher im Jahr grössere Schmelzunterschiede zu beobachten sind, da der Sonnenwinkel eher tief ist und so durch begrenzende Bergen gewisse Orte länger bescheint als andere. Später in der Schmelzsaison stehe die Sonne höher und die Strahlen werden gleichmässiger über das Gebiet verteilt.

Acknowledgments

A very sincere thanks goes to Dr. Tobias Jonas for his excellent support, his highly competent research advices and for giving me an insight into the fascinating subject of snow hydrology during the process of my master thesis.

A special thanks goes to Nena Griesinger, whose first Master student I had the honour to be. No matter whether discussing codes and theories or planning and conducting fieldwork, I highly enjoyed the good teamwork. All the best for your dissertation and the (equal?) important stuff like ski touring on powder days. Take good care of the Lindwurm!

Further I would like to mention Prof. Dr. Jan Seibert for his role as supervisor from the department of Geography at University of Zurich. Moreover, I would like to thank him for sharing his interest and fascination for hydrology with us students.

During my time at the SLF I was very lucky to have a great office mate - Giulia Mazotti. I enjoyed her company in B214 no matter what time of day, good talks and an “occasional” cookie once in a while. Also for helping out with fieldwork and giving valuable input for my master thesis she earns a huge mille grazie! Further I would like to thank the whole snow hydrology team. I always felt welcome to ask questions or discuss stuff with them. Especially I would like to mention Timi’s and Pascal’s unbelievable effort for field work in the early mornings and Sebastian’s coaching for setting up the meteostation. For questions and advice during the final stage of my thesis I was glad to count on support of Dave Moeser and Dr. Adam Winstral.

For non-hydrological questions I was able to ask and discuss matters also with people outside of the group. A special thanks goes to Dr. Joanna Veitinger, who helped me to shed light on rough roughness questions. For excellent support concerning GIS-question I would like to mention and thank Andreas Stoffel. For some valuable advice concerning GPS measurements I would like to mention Dr. Yves Bühler. Also I would like to thank Dr. Lino Schmid for the discussion about radar functionality.

I would like to thank all the people at SLF for making my time in Davos unique. Special thanks goes to Lucie for being my roommate and ski touring friend, to Matschek for showing me the best biking trails around Davos, to Betty for always being motivated to do fun activities, to Alessandro and Lisa for having me at the WG and accompanying me on outdoor adventures, to Pirmin for letting me play soccer and to Hitsch for the good guiding.

When I happened to show my face in Zurich I was lucky to count on the support of many good friends, from which have to be mentioned the members of UNG and the Geographers Ladina, Daniela, Corin, Bernadette and Marius.

Last but not least, a huge thanks goes to my parents for always supporting and encouraging me. But also thanks for the many great adventures, nice times and good laughs spent together.

Content

Abbreviations

CMP	Common Mid Point
C_v	Coefficient of Variation
DEM	Digital Elevation Model
EM	Electromagnetic
HS	Snow Height
ΔHS	Change in HS: Used in this Master Thesis as an equivalent for snow depletion
GIS	Geo Information System
GPR	Ground Penetrating Radar
GPS	Global Positioning System
LiDAR	Light detection and ranging
POW	Peak of Winter
RMSE	Root Mean Square Error
SWE	Snow Water Equivalent
ΔSWE	Change in SWE: Used in this Ma-thesis as an equivalent for snow melt
SD	Standard Deviation
TWT	Two-way Traveltime
VRM	Vector Ruggedness Measure
CVRM	Vector Ruggedness Measure modified with input from Corripio 2003 (See 3.1.2)
S1 to S4	GPR - Transects in the Sertig Valley
M1 to M7	GPR - Transects in the Monbiel Valley

Figures

Tables

1. Introduction

In the Alps a third of precipitation falls in form of snow. During winter snow accumulates and water will be stored until the snowpack melts in spring and the water is released back into the water cycle. The timing and magnitude of melting events is essential in order to predict the amount of melting water that is fed to the rivers of Switzerland. This is of upmost importance when melting events coincide with heavy precipitation events that could cause flooding. Therefore it is important to have accurate snow accumulation / snowmelt models in order to predict the amount of melt water addition to discharge. But not only are such models important for predicting natural hazards but also for industries depending on water, e.g. hydroelectric power plants. In order to develop such models, prior fundamental knowledge about snow accumulation, snow ablation and snow characteristics are an asset.

A substantial part of research in snow hydrology focuses on explaining how snow cover is built up during snow accumulation. In mountainous regions, this is quite challenging because snow cover displays a huge variety of snow height (HS) and snow water equivalent (SWE) and caused by many different processes (e.g. Anderton, White, and Alvera 2002; Egli et al. 2012; Grünewald et al. 2013; Melvold and Skaugen 2013; Trujillo, Ram, and Elder 2009). There is also research done concentrating on snowmelt. For explaining snowmelt patterns there are two different approaches. The first approach regards snowmelt as a homogenous, the second approach as a heterogeneous process. The first approach is based on the assumption that melt will occur equally at a slope- and catchment scale. When considering snowmelt an a heterogeneous process one however assumes that snow melt is dependent on its spatial and temporal location (Egli et al. 2012).

1.1 Motivation

The goal of this thesis is to investigate the snow cover during snowmelt not only based on snow height (HS), but also snow water equivalent (SWE) and compare these findings to previously found results. Many studies so far, mainly used snow height (HS) measures and derived from it snow water equivalent (SWE) estimates (Jonas, Marty, and Magnusson 2009). It is therefore interesting to see whether HS and SWE behave similarly when both measured directly. Measuring HS and SWE at the same time was accomplished by using data from ground-penetrating radar (GPR) surveys, assembled during field campaigns in March and April 2015. The GPR-sensor at use was of type MALÅ ProEx system and belongs to the snow hydrological group at SLF. GPR devices were already used in snow hydrology previously to assess HS measurements and occasionally SWE measurements. However, measuring SWE at different time steps is a rather new concept. Having high spatial resolution data of both HS and SWE may bring more insights to similarities and differences between the two measurement units.

Furthermore, this data set was used to characterize snow cover at the peak of winter (POW) and during ablation. In snow hydrological literature, snow ablation is typically discussed either with a homogenous melt approach or with a heterogeneous melt approach. It was thus examined whether findings of both approaches may be reproduced using HS data from the GPR-measurements and whether it is possible to complement them with GPR based SWE data.

1.2 Research questions

In snow hydrology, GPR-devices have scarcely been used to observe snow ablation. Thus the first research questions is about the performance of such a measurement set up: Do GPR measurements provide good quality HS and especially SWE data? If yes, can they be used to assess differential snow melt?

Using HS and SWE data assessed with the GPR, the following issues are explored: If a homogenous melt is assumed, can the hysteresis approach by Egli et al. (2009, 2012) be confirmed for snow melt season with measured snow heights? Is this effect also visible in the SWE data?

Terrain roughness is known to account for part of the variability in snow cover. Therefoe it was attempted to find out more about the relationship between snow cover or snow melt and the underlying topography at the selected field sites: How does terrain roughness relate to snow cover at POW and during snow ablation?

In order to account for heterogeneous snowmelt, the following research question was posed: Can a spatially variable snowmelt be detected? If yes, what are the causes for this variability?

1.3 Chapter Overview

To be able to answer these research questions repeated measurement campaigns during March and April were conducted at two mountain valleys in the vicinity of Davos. The aim was to gather HS and SWE data of different time steps. This data was then used for the analysis.

In chapter 2, background knowledge over the most important topics relevant for this Master thesis is provided. This includes the topics snow season, GPR basics and terrain roughness.

For the data used in this Master thesis chapter 3 provides an overview of the sources as well as of the programs used to process the data.

In chapter 4 the two fieldsites, Monbiel and Sertig, are presented. Also the meteorological situation during winter 2014/2015 is considered.

Chapter 5 is dedicated to the methods used to assess the HS / SWE data and the terrain, as well as the methods used to analyse them.

The results of the different analyses are summarized and presented in chapter 6 and discussed in chapter 7.

The thesis ends with a conclusion and an outlook.

2 Background

2.1 Snow Season

Seasonal snow coverage consists broadly spoken of two different periods:

- Snow accumulation and redistribution
- Snow melt

Depending on the temperature regime and the altitude, the change from one phase to the other occurs sooner or later. The end of the snow accumulation period marks the peak of winter (POW). Snow cover at this point is the initial condition for snowmelt.

2.1.1 Snow Accumulation

Snow cover is built up continuously from the first snowfall on. During the accumulation period, snow is being accumulated and compressed by compaction. Depending on the vegetation cover, snow is distributed differently (e.g. forest vs. meadow). Open areas are prone to be influenced by snow redistribution by wind. In alpine areas, the complex topography influences inhomogeneous snow distribution even more due to the high spatial variability. Precipitation and wind patterns are very likely to be influenced by topography (Helbig et al. 2015). For example wind may erode snow at exposed sites and deposit it at more sheltered locations. This can lead to ridges being nearly snow free on one side, whereas on the other side the snow pack is some meters deep (Winstral, Marks, and Gurney 2009). Additionally, the smoothing effect of rough terrain leads to a very inhomogeneous HS distribution. It was observed that standard deviation (SD) of HS in rough terrain growth is proportional to mean HS (Egli 2011). Many studies focusing on different factors that lead to inhomogeneous snow accumulation were performed. Different strategies where chosen, ranging from using linear regression to explain snow depth with terrain parameters to using power-law relationships between SD of HS and mean HS (Egli and Jonas 2009; Egli et al. 2012).

2.1.2 Snow Ablation

During snowmelt, water previously stored in the snowpack over winter is continuously released as runoff. Snow ablation can be described both by changing HS and SWE. In the following, when referring to a change of HS the terms “snow depletion” / “snow depletion rates” will be used. For negative changes in SWE, the term “snowmelt” will be used. If both are meant, the term “snow ablation” will be used. It must be emphasized that ultimately only observed changes in SWE can lead to a direct estimation of melt water runoff. Even if changes in HS can very likely be due to melt water runoff, they could also stem from snow compacting due to destructive (temperature) or mechanical (wind) metamorphosis of snow. Nevertheless is it possible to calculate SWE. Observations showed that snow density has a smaller variability than HS. It is thus reasonable to estimate SWE based on many HS measurements and only few snow density measurements (Jonas et al. 2009).

A major driver of snowmelt is the melt energy, which can be computed from the energy balance at a particular point. The elements of the energy balance have the unit Wm^{-2}. The energy balance is described by following equation (Debeer and Pomeroy 2009):

$$Q_m = Q_{LW} + Q_{SW} + Q_H + Q_L + Q_G + Q_P - \Delta U/\Delta t \quad (1)$$

Where Q_m = energy available for snow melt, Q_{LW} = Longwave radiation, Q_{SW} = Shortwave radiation, Q_H= Sensible heat fluxes, Q_L= Latent heat flux, Q_G= Ground heat flux, Q_P = Energy added to the snow cover by precipitation and U = Internal energy of snowpack. Alternatively melt energy can be written as the depth of melt m (Debeer and Pomeroy 2009):

$$m = \frac{Q_m}{\rho h_f \beta} \quad (2)$$

Where ρ = snow density, h_f = latent heat of fusion (0.334 MJ/kg) and β = fraction of ice in snow. As shown by the energy balance, a combination of shortwave and longwave radiation as well as different energy fluxes are the principle causes for snowmelt. The influence of the different parameters is subject of change and is for example depending on the meteorological situation (clear sky, cloudy sky (Anderton, White, and Alvera 2004)), wind (Pohl et al. 2006) or strong sensible heat fluxes (due to change of albedo) caused by snow free patches (Helbig et al. 2015)). Another interesting part of the energy balance is the incoming energy by rain on snow. Energy input caused by rain on snow events can be divided in two parts: The sensible heat energy of water (water is warm and thus contains more energy than snow) but also latent heat set free by freezing of percolated rain water or refreezing of snow previously melted by rainfall (Grenfell and Putkonen 2008). As rain on snow events occur sporadically and are not the overall contributing factor for snow ablation during spring, this energy flux will not be considered further.

Typically the importance of these parameters is related to the stage of the ablation season. For example, as the angle of solar radiation is constantly increasing during the course of the winter season, so does the amount of energy reaching an area. Early in the season, the terrain experiences thus a higher shading effect caused by sheltering of the surrounding mountains. During the course of melting season, solar rays are distributed more uniformly over the terrain. This happens due to a rising solar angle (Anderton et al. 2004). If shortwave radiation was majorly responsible for inhomogeneous melting in the beginning of the ablation season, by the end of ablation season sensible heat flux by snow free patches grows to be more important (Anderton et al. 2004; Helbig et al. 2015).

Some studies also assess accumulation patterns based on linear (Pomeroy et al. 2003) or power law relationships (Egli and Jonas 2009; Egli et al. 2012) between SD of HS and mean HS. The approach from Egli and Jonas (2009), Egli et al. (2012) proved to work well at different scales with data collected in in the alps. However when applying this approach to catchments worldwide this relationship does not always exist (Grünewald et al. 2013; Helbig et al. 2015).

When observing ablation processes in the mountains, it becomes clear that there must be a difference in melting rates at extreme opposite slopes, e.g. between southerly and northerly exposed slopes (Debeer and Pomeroy 2009). If either more homogenously exposed slopes or bigger areas where all expositions appear evenly are investigated, the question arises whether inhomogeneous melt rates matter for explaining snowmelt. Accordingly, there are two different approaches currently used in snow hydrology: Investigation of snowmelt assuming either homogeneous or inhomogeneous melt.

Looking at studies using the heterogeneous snow ablation approach, (variability in) snow melt is tried to be explained by either terrain parameters or processes like heat fluxes or prevailing wind systems (Debeer and Pomeroy 2009; Grünewald et al. 2013; Winstral and Marks 2014).

As e.g. Egli (2012) could not find a correlation between terrain and snowmelt patterns at his field site Wannengrat, he tried to use a homogenous approach to describe melt. As already shown in Egli & Jonas (2009), during snow ablation season mean HS is constantly decreasing while SD of HS stays at approximately the same level until snow vanishes at the vast part of the area. Based on this observation and the presumption of homogenous melt, they were able to predict snow melt for the whole fieldsite based on reference snow measurements taken at a flat site nearby (Egli et al. 2012). If a homogenous melt rate is assumed, the importance of initial snow distribution grows, because variability of HS at POW will have the most significant impact on snowmelt patterns.

In summary, snowmelt rates and patterns may vary within a catchment, even though in recent studies only part of the snowmelt variability was explainable with terrain variables (Debeer and Pomeroy 2009). However, very solid results were gained by assuming homogenous snowmelt and simple relationships like the ratio between the mean of HS and SD of HS. It was proved possible to model snow ablation without actually taking account of topography at certain scales and regions (Egli et al. 2012).

2.2 GPR Basics

2.2.1 Electromagnetic Background

The physical foundation of GPR-measurements is built upon the electromagnetic (EM) theory. The relationship between electric and magnetic fields is summarized by Maxwell's equations and the constitutive equations. Basic variables that are needed to describe a material's response to an EM field are electrical conductivity σ, dielectric permittivity ε and magnetic permeability μ. Electrical conductivity σ describes the free charge movement within an electric field. Dielectric permittivity ε describes the material's property reaction to an electric field. Magnetic permeability μ describes the magnetic property for a material (Annan 2009).

2.2.1 GPR Measurement System

GPR-systems consist of a component that emits EM waves and a component that receives the response. In homogenous underground, electromagnetic waves have a straight travel path. At boundaries of layers with different dielectric properties, parts of the waves are reflected (Annan 2009). The reflector depth is assessed by measuring the two way travel time (TWT) that means the time needed for an EM wave to travel from the transmitter to the reflecting layer and then to the receiver, influenced by the relative permittivity of snow / media.

It is therefore possible to investigate the snow cover depth with a GPR, since snow cover has very different electromagnetic properties than the ground underneath and EM waves will therefore be reflected at the interface between snow and ground (Bradford, Harper, and Brown 2009). The electromagnetic waves have usually a frequency between 10 MHZ and 10 GHZ. In wet snow, the higher the frequency, the higher is the resolution, but the less deep the wave penetrates. The emitted free waves penetrate the surface and eventually reach the receiver, influenced by transmission, reflection and backscattering processes. The GPR result is then displayed as a radargram, which is in fact a set of traces. One trace equals one single GPR measurement (Annan 2009).

The antennas were set up in a multi-offset setup. This means that the principle of common-offset measurements is combined with the advantages of the common midpoint setup. Common offset setups contain a single transmitter – receiver pair that is placed in a known distance. Common mid-point (CMP) setups on the other hand are based on measuring TWT for the same spot multiple times with different antenna separations each time. All used antenna separations yield a common midpoint. For this, both transmitting and receiving antennae must be moved simultaneously in identical distances. In general, no assumptions for reflector depth or relative permittivity have to be made, since both velocity and HS can be determined. As a consequence however, a CMP surveys proved to be rather time intensive and can thus only be applied for limited ranges. This is where the solution of a multi-offset setup comes in. Multiple transmitter-receiver pairs, sitting on a sledge, are used that have a fixed separation though the same common-mid point. Despite being less accurate than CMP-measurements because having multiple unknown TWT offset values, the multi-offset yields the potential to assess average relative permittivity and water content. The only disadvantage compared to common offset measure is the longer measurement time (Annan 2009).

2.2.3 Applying GPR to Snow Hydrology

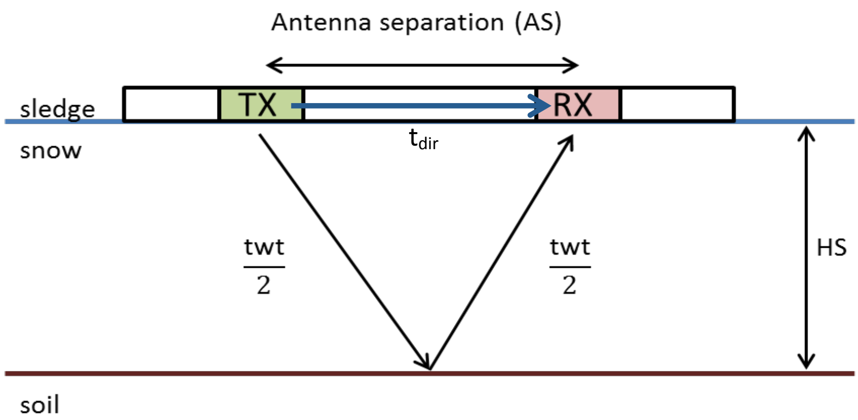

Figure 1. Conceptual GPR setup.

Figure 1 shows a conceptual radar setup in snow. The sledge with transmitting and receiving antennae lies on snow and sends EM waves to the ground that are reflected at the snow – soil interface. TWT can be calculated from the distance travelled by the EM wave and is divided by the velocity of the EM wave in snow (Gustafsson, Sundström, and Lundberg 2012):

$$TWT = \frac{2\sqrt{(\frac{AS}{2})^2+HS^2}}{v_{snow}} \tag{3}$$

In a multi-offset approach the different antennae separations cause different travel paths and hence a differing corresponding TWT. This results in a hyperbola with antenna separation on the x-axis and TWT on the y-axis. If the hyperbola is fitted to reflection a depth-velocity model is obtained that can be used to calculate HS as well as v_{snow} (Takahashi et al. 2007).

$$v_{snow} = \frac{1}{\sqrt{\varepsilon' \mu_0}} \tag{4}$$

When looking at radar wave propagation in snow a difference between dry and wet snow has to be made. V_{snow} depends on real effective permittivity ε' and magnetic permeability μ. In snow μ = permeability of free space = μ_0 is valid. In dry snow real effective permittivity ε_{snow} is a function of snow density, whereas in wet snow real effective permittivity ε' is a function of snow density and liquid water content (LWC). In Figure 2 the effect LWC in the snow pack on EM velocity is shown

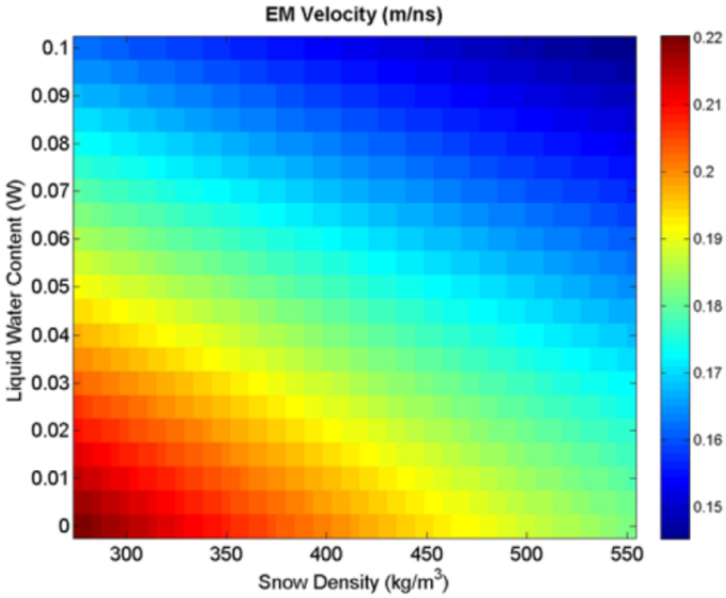

Figure 2. Velocity of the EM wave as a function of snow density and LWC (Figure from Bradford et al. 2009).

Because measurements took place in the ablation season it was assumed that liquid water was present in the snow cover. Therefore, the formula of Looyenga (1965) was used to calculate SWE. This formula (5) converts real effective permittivity ε_{snow} into heterogeneous mixtures (Looyenga 1965).

$$\sqrt[3]{\varepsilon_{snow}} = \theta_{ice}\sqrt[3]{\varepsilon_{ice}} + \theta_{water}\sqrt[3]{\varepsilon_{water}} + \theta_{air}\sqrt[3]{\varepsilon_{air}} \quad (5)$$

θ stands for the volumetric content of air, ice and water in snow. ε_{ice}, ε_{water} and ε_{air} are physical constants that are known for specific radar frequency and temperature. Even though studies were made to estimate LWC directly from GPR data (Bradford et al. 2009; Sundström, Kruglyak, and Friborg 2012), in this thesis LWC was derived from manual measurements. Knowing LWC, the relationship $\theta_{air} = 1 - \theta_{water} - \theta_{ice}$ (6) makes it possible to calculate the volumetric content of ice and water (Sundström et al. 2012).

Using the volumetric contents of ice, water and air snow density can be derived (Sundström et al. 2012) as shown in equation 7:

$$\rho_{snow} = \theta_{ice}\rho_{ice} + \theta_{water}\rho_{water} + \theta_{air}\rho_{air} \quad (7)$$

Based on the assessed snow density SWE can then be calculated using HS, snow and water density (Lundberg, Richardson-Näslund, and Andersson 2006):

$$SWE = \frac{HS\rho_{snow}}{\rho_{water}} \quad (8)$$

2.3 Terrain Roughness

Terrain roughness or ruggedness is understood and calculated in a variety of different ways. Hobson (1972), states: *«A single concise definition of surface roughness is probably impossible».* Very coarsely terrain roughness can be understood as the variability of a topographical surface at a given scale (Veitinger, Sovilla, and Purves 2014). Rough terrain can be seen as the opposite of smooth terrain. There are many different terrain roughness calculation techniques. In general they can be divided into profile based and array based techniques (Grohmann, Smith, and Riccomini 2011). In 2.3.2 and 2.3.3 these will be shortly discussed. In literature the terms "roughness" and "terrain ruggedness" are often used as synonyms, therefore this will be done here as well. Generally, it will be spoken of terrain roughness but for the case of a roughness measure called vector ruggedness measure, an exception will be made.

In the following, the importance of terrain roughness with regard to snow hydrology is illustrated and current roughness approaches are presented.

2.3.1 Importance of Terrain Roughness

During the snow accumulation season, snow is stacked up on the prevailing landscape. If the landscape is smooth, snow will accumulate with an even HS over the whole area and will leave a winter surface that is very similar to the summer surface (without any other influences, e.g. wind). However, if the landscape is rough, snow will smoothen the surface and will change it dramatically compared to the summer surface. Figure 3 illustrates how the first snowfall hardly changes the summer surface, but with increasing accumulation the summer surface will be more and more smoothed out. Thereby, terrain roughness may act as snow trap (Helbig et al. 2014) and also plays a role in avalanche formation and dynamics (Veitinger et al. 2014). Looking at terrain smoothing from another side, it can be seen as creating a snow cover with a very high HS / SWE variability, which can be a challenge to model (Helbig et al. 2014). To better understand accumulation patterns and to also be able to explain melting pattern a suitable roughness measure was looked for.

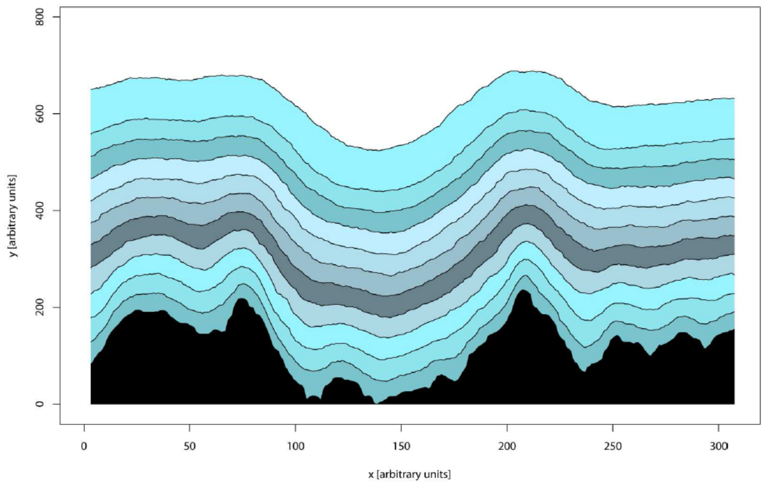

Figure 3. Modelled terrain smoothing caused by snow accumulation. The black underground symbolizes rough terrain, whereas blue layers represent snow fall events (Figure from Egli 2011).

2.3.2 Profile-Based Terrain Roughness Techniques

One way to assess roughness of a terrain is to calculate how rough a, mostly field-surveyed, profile is. It is therefore a 1D approach that does only account for roughness in one direction. The result can then be either visualized as a grid, drawn as a profile or presented as summary statistics (Grohmann et al. 2011). Profile-based terrain roughness measures may include SD of elevation or slope, or more mathematical solutions like applying fractals or Fourier analysis to the surface (Olaya 2009). Fractals have already been used to relate mountain snow distribution to an elevation gradient as well as to roughness (Lehning, Grünewald, and Schirmer 2011). Applying profile-based terrain roughness is suitable for the measured data, because the measured transects are also linear and not areal data. In general, profile-based terrain roughness techniques provide limited information that may neglect some of the topography's variability. When terrain roughness should not only identify rougher over smoother terrain but also be able to quantify roughness, array-based solutions will provide better results (Grohmann et al. 2011).

2.3.3 Array-Based Terrain Roughness Techniques

Since array-based roughness measuring methods depict the landscape more exactly, the aim was to find a method that reflects the field sites correctly and logically. Hobson (1971) emphasized that: *"An optimal roughness parameter should be able to describe variations from very small scale to larger scale."* As the chosen fieldsites are not within highly rough terrain (e.g. rockfaces) it was of interest to find a measure that identifies small-scale differences. Since roughness is defined by varying surface and not by magnitude of slope it is crucial that roughness should not correlate with slope. Most of the widely used roughness measures rely on a DEM as a starting point.

In order to give an overview over standard roughness measures, three different measures are shortly summarized. For evaluating roughness, it is essential to know how the terrain looks like in reality. Also, it is crucial that roughness measures distinguish between steep and rough slopes since steep slopes may also be smooth (Sappington, Longshore, and Thompson 2007). For Grohmann et al. (2011) three elements were crucial for roughness to be represented: Overall impression, depiction of urban and forested areas and correctly illustrating scarps as smooth despite being steep. To be able to focus on one roughness measure hereafter a preliminary evaluation and selection is presented here shortly.

A quite basic roughness measure is to calculate the SD of a terrain variable raster for a grid cell using a predefined moving window (e. g. 3*3). In their review, Grohmann et al. (2011) found SD of slope to be a suitable method for terrain analysis, based on sensitivity to rapid slope value changes and highlighted boundaries between urban and forested areas. Also the scarps are depicted as smooth as they should be. Another possibility is to use the SD of curvature or elevation. If using SD of elevation values, these should be detrended first since otherwise there will be a high correlation with slope. Curvature is the second derivative of slope. In general SD of slope as well as SD of curvature perform well, especially for detecting linear features such as streams. SD of curvature is prone to highlight features prominent to dominant slopes, while SD of slope tends to assign low values to the top of ridges, but high values to valley bottom (Brubaker et al. 2013). Despite being evaluated as suitable roughness measures in general, they do not characterize the fine roughness of terrain at the field sites well enough.

The terrain ruggedness index (TRI) and the topographic position index (TPI) are further possible ways to assess terrain roughness (Revuelto et al. 2014; Sappington et al. 2007). While TRI uses the mean of the absolute elevation change for a grid cell in a 3*3 neighborhood (Sappington et al. 2007), TPI takes the difference between the value of a grid cell and the mean value of it eight neighboring cells (Revuelto et al. 2014). Despite Revuelto et al. (2014) achieved stunning results, TPI did perform very badly for the fieldsite terrain. TRI depicted the roughness of the terrain quite accurately, but proved to be highly correlated with slope.

As a third approach the vector ruggedness measure (VRM) must be named. VRM is a way to describe terrain roughness based on the variability between unit vectors normal to the surface area, illustrated in Figure 4. VRM was developed by Sappington et al. (2007). It is based on the idea of using vectors to describe surface changes as initially proposed by Hobson (1972). Also Grohmann et al. (2011) take this method (as “vector dispersion”) into account. They found that this method has a good sensitivity to local variations in elevations, both in vegetated and urban areas. Furthermore, scarps are shown as smooth areas proving that this method is able to differ between steep slope and rough terrain. Recently Veitinger et al. (2014) applied this method in order to assess the snow cover introduced change of terrain roughness with the aim to investigate the role of terrain roughness on avalanche dynamics. When applied to the fieldsite terrain, results were very convincing. Furthermore, no correlation between VRM and slope is visible. Therefore it was decided to use VRM for further analyses. It will be discussed more closely in chapter 5.1.

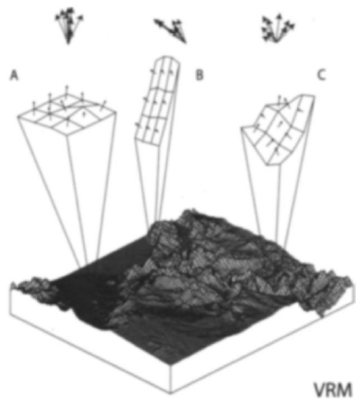

Figure 4. Principle of VRM: Smooth terrain includes both flat and steep slopes (A and B) that show a small vector dispersion. Rough terrain in contrary shows a large vector dispersion (Figure from Sappington et al. 2009).

3 Data and Software

For this master thesis, data from different sources as well as multiple software was used. They will be listed and described shortly in the following section.

3.1 Data

Data used in this Master Thesis stem from the following three sources.

- Fielddata
- Geodata
- Meteodata

3.1.1 Fielddata

During several measurement campaigns in spring 2015, snow data was collected in two different alpine valleys. For the snow measurement, a GPR (MALÅ ProEx system) mounted on a sledge was used, as well as manual measurements were undertaken in order to calibrate and validate GPR measurements. Measurements were taken along transects and replicated multiple times with a time lag in between, in order to capture some of the snow ablation processes during the ablation season. More information on the field sites will follow in chapter 4. The measurement set up will be explained in chapter 5.2.

The transects were georeferenced using GPS data collected during the measurements. Each transect was registered once with a handheld GPS. Transects in Sertig valley were recorded with a differential GPS (Trimple GeoXH, Geoexplorer 6000 series). The accuracy of <1m was made possible thanks to the SWIPOS station in nearby Davos. For Monbiel a Garmin GPSmap 62st was used that has, thanks to reception of EGNOS data, an accuracy of <3m.

Additionally, every measurement from each measurement day was traced with a GPS (BU-353, accuracy 3m) connected directly to the GPR computer. The person pulling the sledge on the right side during the campaigns always carried the GPR computer. Therefore these GPR Tracks deviate from 1-2m from the tracks from the handheld GPS. Accuracy of the GPR-connected GPS was also assessed by the reception of EGNOS data.

Comparing hand held GPS tracks and GPR-connected GPS tracks revealed that the tracks usually followed a similar route. It was noticed that the GPR-connected GPS sometimes had issues in finding the right location, as shown by evident outliers. Zooming in closer, it is also visible that the GPR-connected GPS is not always on the right side of transects, where it theoretically should have been.

Due to these slightly unreliable results from the GPR-connected GPS, it was decided to use only data from the more accurate and reliable differential GPS for the Sertig valley. Since in Monbiel valley two GPS-system with a similar accuracy were used, it was not equally easy to make a decision which

GPR-tracks to choose. After observing GPS-tracks closer it was decided to take the Garmin tracks due to its placement on the sledge. There was one exception. On transect 4 all GPR-connected GPS tracks showed a different pattern from the Garmin GPS. For the two more similar GPR-connected GPS tracks a centre line was drawn (using “Collapse Dual Lines to Centerline” tool in Arc GIS). To take the offset between sledge and GPS device into account, a buffer of 2m was wrapped around the center line. Consequently, the Garmin GPS track was adjusted to the left side of the buffer.

The number of synchronized GPR-measurements per transect was then used to create corresponding points along the measured GPS line using “Line to Point tool” in ArcGIS. XY-coordinates where added to theses axes. For each point, terrain information (elevation, aspect, slope, roughness measure) was extracted using the ArcGIS “Sample” tool. Those points were then transferred to R to be joined with the corresponding HS and SWE measurements of the field days.

A basic rule to estimate grid cell size according to accuracy of GPS is to take the accuracy of GPS as the radius of a circle that describes the “error area” (Hengl 2006). This resulted in a theoretical minimum cell size of 6m for Monbiel and 2m for Sertig. For Sertig it was possible to use the original LiDAR data (SwissAlti 3D). Under the premise that terrain would not deviate crucially within 3m of each transect side, results of SwissAlti 3D were used for Monbiel as well.

3.1.2 Geodata

In order to calculate terrain parameters, it is crucial to have a good digital elevation model. For this Master thesis swissALTI^{3D} (version of 2014) by Swisstopo was used. It is a derivate from the database for elevation products DTM-TLM by the Bundesamt für Landestopographie swisstopo. Elevations below 2000m a.s.l., are based on a digital terrain model achieved by LiDAR measurements. In areas above 2000m a.s.l., there is new elevation data derived from stereoscopic autocorrelation derived from aerial images recorded by swisstopo (flight years 2008 until 2011). Every six years changed elevations will be replaced.

For the overview maps the newest version (Q4 2014) of ”Landeskarte 1:25’000“ by swisstopo were used.

3.1.3 Meteodata

For each field site, a meteostation of the snow hydrology group was built up in the beginning of winter. Among others HS, air temperature and surface temperature was measured and then used to evaluate the meteorological conditions of the ablation phase.

To be able to compare this winter to precedent ones, data from IMIS stations as well as observer data (both “SLF inhouse” products) were used. IMIS is a network of meteostations all over Switzerland that is complemented by observer data measured manually by observers.

3.2 Software

Following software was used for analysing and calculating data:

- R: Version 3.1.2
- Matlab: Version R2013a
- ESRI ArcMap (Licence Key: ArcInfo): Version 10.0
- ReflexW: Version 7

3.2.1 R

R is a statistical, code based open source program. It was used for most of the data analyses, plotting and also evaluating correlations between terrain parameter and (changes in) snow cover. Furthermore, the roughness measure VRM and CVRM were calculated using R. To be able to calculate VRM and CVRM the package ‘raster’ and ‘insol’ were used.

3.2.2 Matlab

Matlab is a commercial software using codes to analyse and plot data. Tobias Jonas implemented GPR4snow, the program used to calculate HS and SWE from the radar data, in a Matlab environment. In addition to calculate HS and SWE data from the radar measurements other steps like the synchronisation of transects and the calculation of RMSE between manual and GPR-measurement were also calculated with Matlab. MetDataWizard, the program used to display and clean up meteodata, is based on a Matlab script.

3.2.3 ESRI ArcMap

ArcMap is a powerful commercial GIS-software. It was used for most of the terrain calculations. For calculations ArcMap did not provide a tool (e.g. terrain roughness), it was decided to take R.

3.2.4 ReflexW

In ReflexW the first steps of the post-processing of the GPR-data was made. Radar data is displayed in a radargram. Raw GPR data may be enhanced tools like applying filters or a migration. Using the radargram, the upper and lower snow boundary was defined manually using the “pick” option.

4 Fieldsites

For the HS and SWE measurements two mountain valleys in the vicinity of Davos were selected: The valley behind the village Monbiel, close to the municipality Klosters and the Sertig valley near Frauenkirch Davos. The two field sites were already selected end of November and early December, because it is good to know what lies underneath the snow and to get a general idea of the terrain without snow. Following conditions had to be met by a potential fieldsite:

- For the use of a GPR it is crucial what ground type is underneath the snow to have valuable measurements. There are several underground types that do not make a suitable underground, e.g. Alpenrosen, a very bushy alpine plant, may trap air which leads to a very scattered result. Therefore, this study looked for alpine meadows or terrains with a similar underground.
- The fieldsites aimed at covering a variety of expositions and terrain shapes. Because of valley orientation and accessibility it was not possible to set transects evenly on each exposition / terrain shape.
- Because of staff availability and material transport, the measurements sites needed to be in the vicinity of Davos and accessible by car.
- Fieldsites must not be located close to possible avalanche run out terrain. On one hand this was for safety reasons. Furthermore, it does make little sense to compare measurements of avalanche debris to normal snow cover. Additionally, avalanches going down in between measurements would falsify the results.
- Also little or no human presence was an asset since the single transects where too long to mark them (e.g. put a fence around) in order to keep people from stamping through the snow cover and hence destroying the transects.
- In order to survey more than one valley it was essential to have a sufficient elevation gradient between them to have delayed melting periods between the fieldsites.

4.1 Monbiel

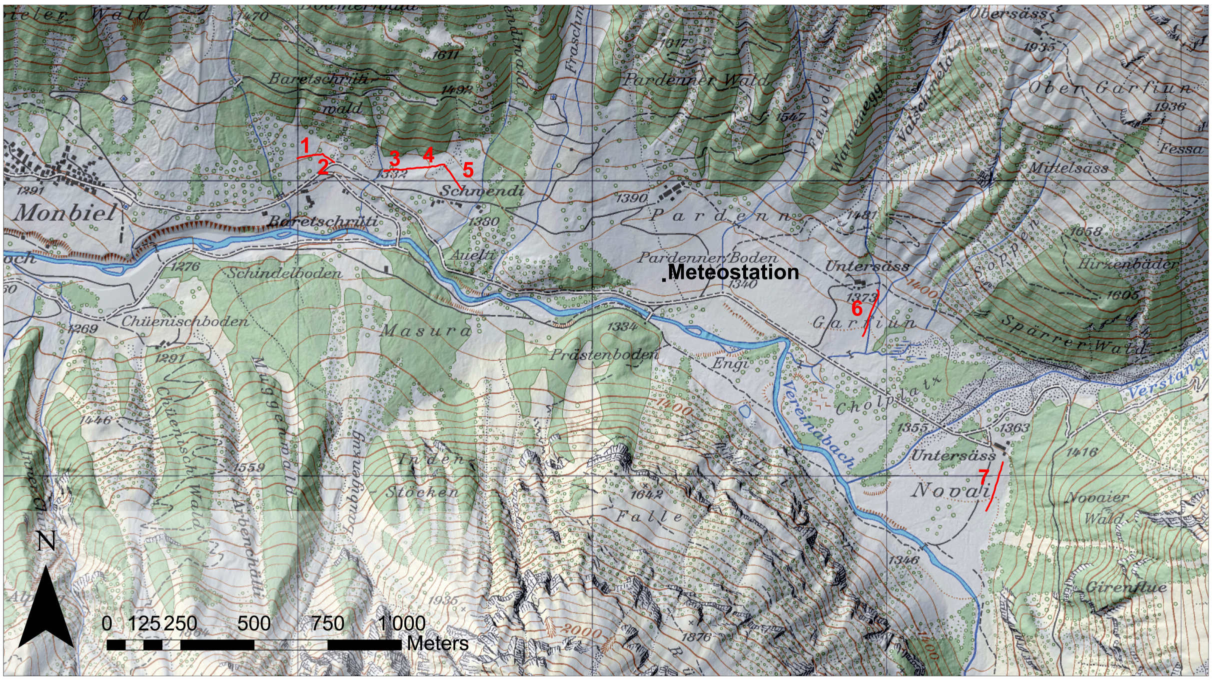

Figure 5. Overview of the fieldsite Monbiel. The red lines show the location of the measured transects. Also the meteostation at Pardenner Boden is shown.

Monbiel is a small village eastwards of Klosters. Transects lay between Monbiel and Novai at the ending of the Vereina valley (see Figure 5). Transect elevation ranges from 1326 – 1374 m a.s.l.. The transects have a southerly exposition ranging from west to southeast. Measurements where taken at 7 different transect, further referred to as M1 to M7. Initially there were two more transects planed, which had to be cancelled due to meteorological conditions in the planned time frame. In average the transects are about 100m long. Slope angles are ranging between 0.5° and 18.5° and are on average 5.5° (see Figure 6). This is little compared to slope at higher elevations, but accessing and measuring steeper slopes with the GPR is rather difficult. Vegetation type is a mixture between alpine meadows and forests. Higher up there are also rock faces visible. Rougher as well as smoother terrain was chosen.

Fieldwork took place from 09.03 – 21.03.2015. In order to have more accurate reference measurements (also for future modelling of radiation) a meteorological station was installed at Pardenner Boden in the beginning of January. From January to April the meteostation at Pardenner Boden measured the most frequent wind direction to be southeast, though ranging from west to southeast (see Figure 6). The mean temperature was -1°C, with extrema at -17°C and +17°C.

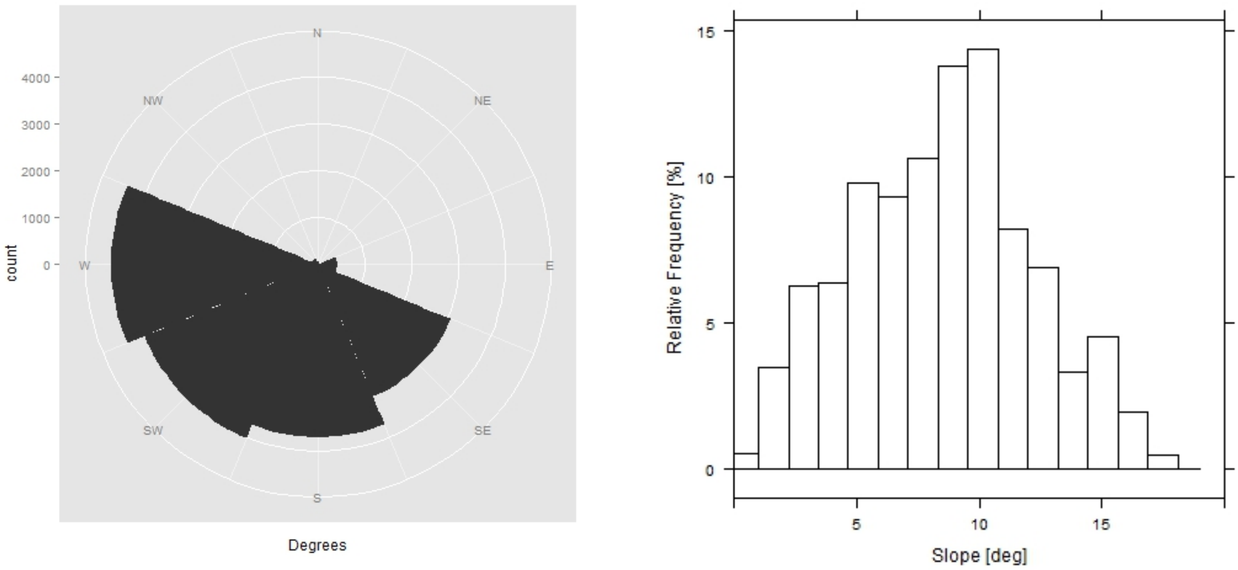

Figure 6. Distribution of aspect and slope angle for transects at Monbiel.

4.2 Sertig

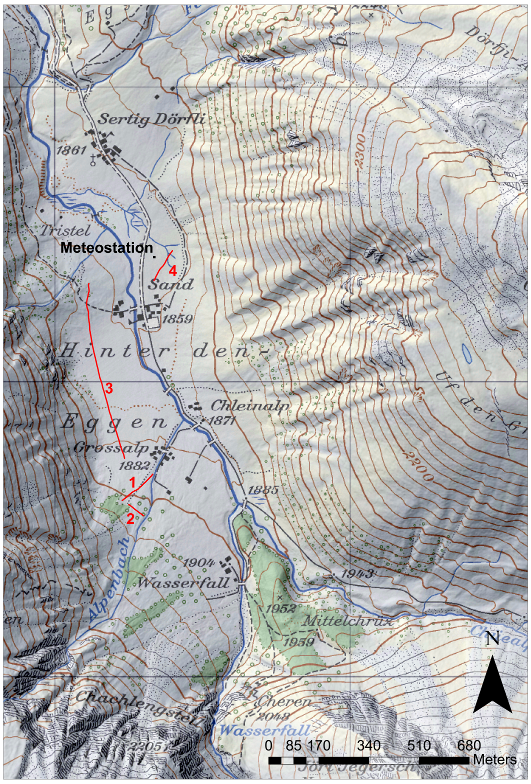

Sertig is a valley southeasterly from Frauenkirch and Clavadel. Transects at Sertig valley range from 1853 – 1919m a.s.l.. The transects are predominantly northerly exposed, ranging from northwest to south east (see Figure 7, 8). Here measurements were taken at four different transects, called thereafter S1 to S4. S1, S2, S4 are in average also ca. 100m, whereas S3 was around 600m. The average transect slope is 5.5°, while the minimum is at 0.5° and the maxima is at 18.5°. Transects at Sertig are therefore slightly flatter than in Monbiel.

Fieldwork was done between 08.04.2015 and 24.04.2015. Mean temperature during the season (taken into account 01.01. – 30.04.2015) ranged from -20°C and +12°C. The mean lay at -3°C.

Figure 7. Overview of the fieldsite Sertig. The red lines show the measured transects. Also the Meteostation at Sertig is shown.

The fieldsite at Sertig has the colder temperature regime than the fieldsite in Monbiel. This is most probably due to the elevation difference from about 500m (assuming per 100m elevation difference a change of 0.8°C this would mean that the two valley show a similar, depending on their elevation, temperature regime). Wind during the season was prevailing from a southeastern direction and ranged from south to east.

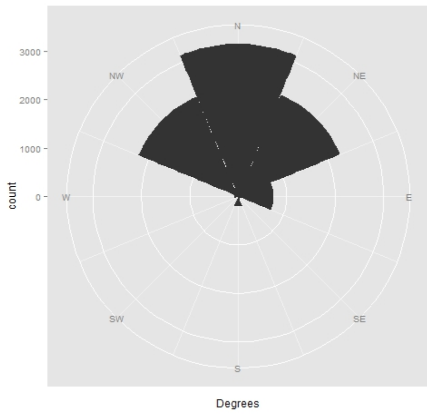

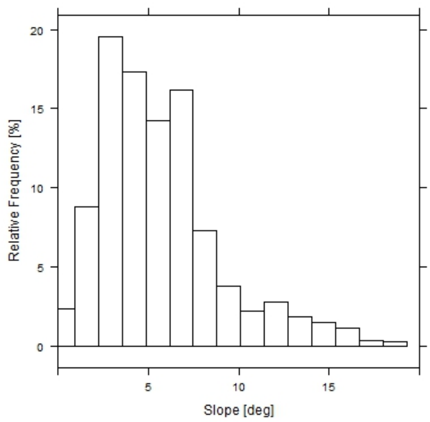

Figure 8. Distribution of aspect and slope angle for the transects at Sertig.

4.3 Meteorological Overview

Looking at IFKIS data from this season and observer data from Davos (Figure 39) and Klosters (Figure 40), it becomes evident that apart from few small peaks, the snow cover depth was below average during season 2015. After a short snow fall in October, there was only little new snow until the end of December / early January, when the snow cover started to build up. Looking at the station data of the two field sites (see Figure 9 and 10), the snow cover grew until the beginning of March, when a first melting period took place. At Klosters as well as at Monbiel, this was when already a lot of snow melted. In the beginning of April there was again snowfall that increased snow depth a little bit in Monbiel. In Sertig, less snow melted during the first melting period, thanks to the snow fall by the end of March / early April, the snow depth nearly increased back to the former HS. For Monbiel valley, the POW is in the beginning of March, while for Sertig the second peak is taken as POW when measurements started. As expected, snow ablation started simultaneously with the increase in temperature. When covered by snow, the soil temperature in Monbiel is higher than in Sertig. This is probably due to the fact that soil in Monbiel was not frozen by the time of snow accumulation, whereas soil in Sertig was already frozen and had therefore a lower temperature. Another explanation would be a slight inaccuracy of the measurement devices. Precipitation was measured as well, but since the rain gauge was not heated, it must be considered to be a rough estimate of precipitation during winter. Looking at the ablation season it becomes interesting though, when there was precipitation as rainfall. It shows, for example, the heavy rainfalls after the last campaign in Monbiel, which were the reason why measurements were stopped then.

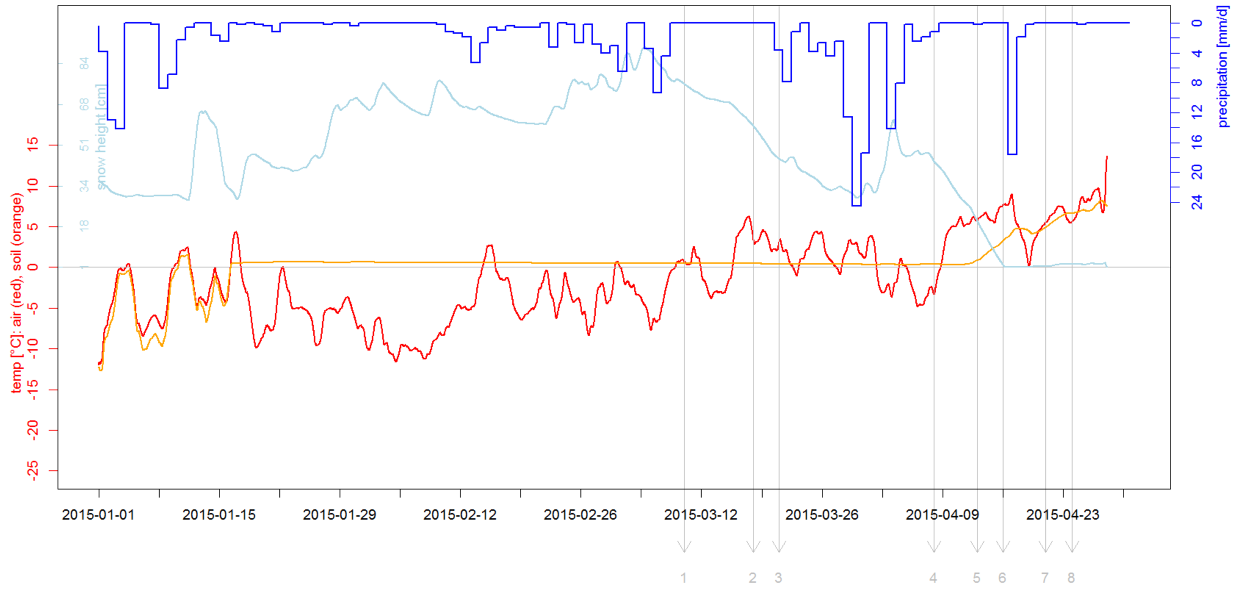

Figure 9. Metorological overview of the winter 2014/2015 (January - April 2015) for the station at Pardenner Boden. Legend: 1 = 10.03.2015, 2 = 18.03.2015, 3 = 21.03.2015, 4 = 08.04.2015, 5 = 13.04.2015, 6 = 16.04.2015, 7 = 21.04.2015, 8 = 24.04.2015.

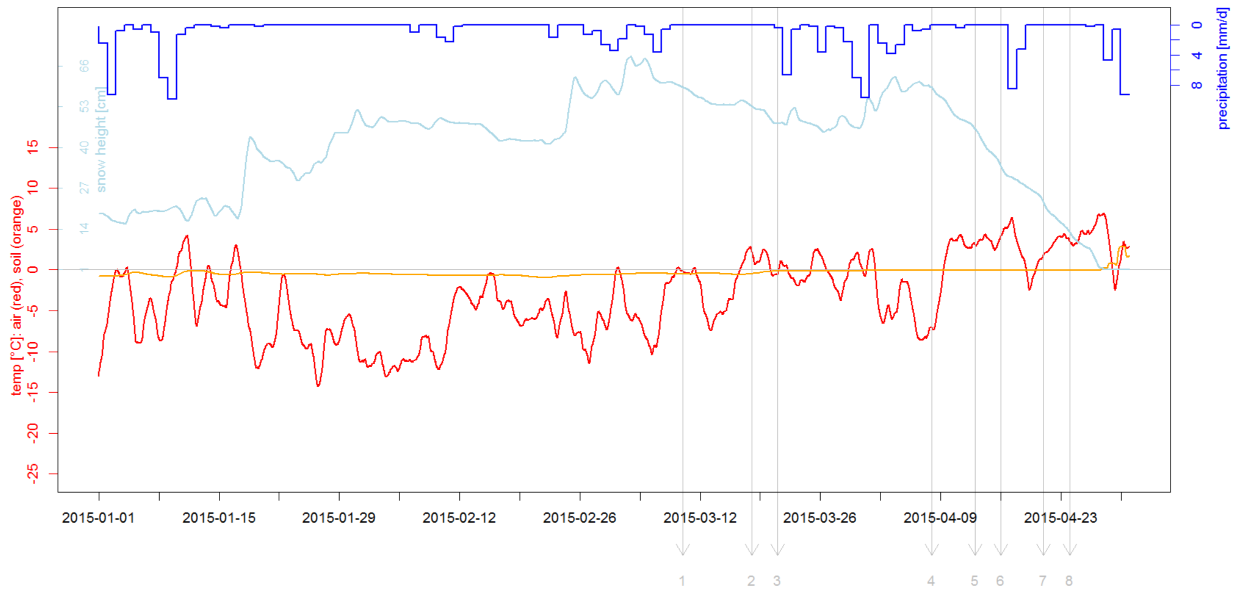

Figure 10. Meteorological overview of the winter 2014/2015 (January - April 2015) for the station at Sertig. Legend: 1 = 10.03.2015, 2 = 18.03.2015, 3 = 21.03.2015, 4 = 08.04.2015, 5 = 13.04.2015, 6 = 16.04.2015, 7 = 21.04.2015, 8 = 24.04.2015.

5 Methods

5.1 Terrain Roughness

5.1.1 1D Solution

The reason why applying the 1D solution is following: By using snow depth at POW roughness with snow cover as well as without snow cover can be derived for the transects. The two basic input values are the elevation above sea level that is derived from the 2m SwissAlti3D dataset from Swisstopo and the initial HS. Based on Figure 19 further explained in 5.3 transects were cut into slices of approximately 20m length. To calculate profile-based roughness of winter and summer surface, the SD of elevation was used. For summer surface elevation was detrended first, while for winter surface HS at POW was added and then detrended prior to calculating SD. This was done for each transect slice. Finally, summer roughness was plotted against winter roughness.

5.1.2 Array-based solution

Assessing terrain roughness in a 1d way makes a lot of sense when applied to evaluate a line. However, terrain roughness is an area feature, therefore usually array-based algorithms are applied. To be able to characterise the entire fieldsite, terrain roughness was also calculated for the whole area of the fieldsites. As described in chapter 2.3 there are many different measures to describe terrain roughness. For our fieldsites, VRM proved as a very suitable method. In a second step, it was further adapted to a measure more sensible towards changes in terrain, hereafter referred to as CVRM. Both methods were calculated using R. To calculate VRM a script by Jochen Veitinger was used. The R script for CVRM is a combination of the VRM script and calculations from the R-package "insol". The DEM used was SwissAlti3D with a 2m resolution (see chapter 3.1.2).

Applying VRM, slope and aspect were calculated first, taking either the magnitude (slope) or direction (aspect) of the steepest elevation gradient between the cell centre and its eight neighbouring cells. In order to calculate slope and aspects algorithm of Zevenberg and Thorne were used (Burrough and McDonnell 1998). In the following calculating slope and aspect for a 3*3 cell raster (Figure 11) with the cell centre "e" is shown.

a	b	c
d	e	f
g	h	i

Figure 11. "Dummy" - Raster

First the maximum change rate in both x- and y-direction have to be calculated. Algorithm for change in x-direction is given by equation 9:

$$\frac{dz}{dx} = \frac{(c + 2f + i) - (a + 2d + g)}{8 * x\_cellsize} \quad (9)$$

While the algorithm for change in y-direction is:

$$\frac{dz}{dy} = \frac{(g + 2h + i) - (a + 2b + c)}{8 * y\_cellsize} \quad (10)$$

Based on those these two equations slope as well as aspect can be derived. For terrain roughness calculation slope in degrees was used. Following formulas describe slope α (Burrough and McDonnell 1998).

$$\alpha(degrees) = \tan^{-1}\left(\sqrt{(\left[\frac{dz}{dx}\right]^2 + \left[\frac{dz}{dx}\right]^2)}\right) * (\frac{180}{\pi}) \quad (11)$$

The result of the aspect calculation is given as clockwise degrees of the compass directions (0° - 360°, 0° and 360° being exactly north). Flat surface that have no direction are given the value -1 in ArcGIS. Aspect β is calculated using following formula (Burrough and McDonnell 1998):

$$\beta = \tan^{-1}\left(\frac{\frac{dz}{dy}}{\frac{dz}{dx}}\right) \quad (12)$$

Calculating slope and aspect using a 3*3 neighbourhood keeps the influence of out layers low, since more cells have an influence. Consequently, there will be a slight smoothing effect (Corripio 2003).

In a second step (Figure 12) the x, y, z components of a unit vector normal to the surface of the cell are constructed using slope and aspect (Sappington et al. 2007).

$$z = 1 * \cos(\alpha) \quad (13)$$

$$xy = 1 * \sin(\alpha) \quad (14)$$

$$x = xy * \cos(\beta) \quad (15)$$

$$y = xy * \sin(\beta) \quad (16)$$

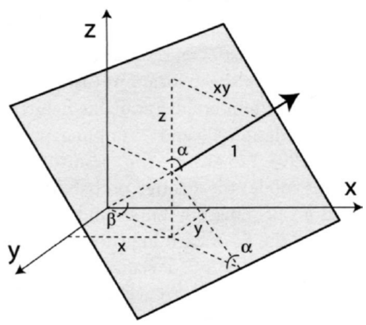

Figure 12. Calculating a vector normal to the plane of a grid cell in order to calculate VRM (Figure from Sappington et al. 2003).

By summing up the single components of the centre pixel and its eight neighbours a resultant vector is calculated (see Figure 13). Neighbourhood size may be defined as big as wished (Veitinger et al. 2014), in this case a 3*3 moving window size is applied. The resultant vector is finally normalized by dividing by the number of grid cells n and subtracting the result from 1 (Sappington et al. 2007).

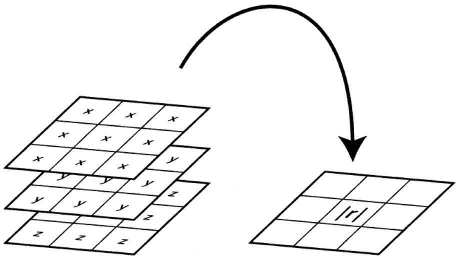

$$|r| = \sqrt{\left(\sum x\right)^2 + \left(\sum y\right)^2 + \left(\sum z\right)^2} \quad (17)$$

$$R = 1 - \frac{|r|}{n} \quad (18)$$

Figure 13. Calculating resultant vector by summing up vector components (Figure from Sappington et al. 2007).

The roughness degree will be given for each grid cell of the DEM, where 1 indicates extreme roughness and 0 no roughness. It is observed that for a bigger moving window than 3*3 the terrain will be smoothed substantially (Sappington et al. 2007; Veitinger et al. 2014).

Although providing very satisfying results, there was a wish to further enhance small-scale variability. Today, many ready-made tools (e.g. ArcGIS, R raster package) calculate slope and aspect using a 3*3 window. The reason for this is that with an eight-pixel neighbourhood, outliers or measurement inaccuracies have less effect on the result. However, using eight neighbouring cells also has a smoothing effect (Corripio 2003). Moreover, calculating slope or aspect based on an 8-neighbourhood method results in an actual area that is 1.6 – 2 times larger than the original pixel (Hodgson 1995). Therefore, other ways of calculating slope and aspect were considered, one of them being to compute terrain variables only based on four grid cells (Hodgson 1995). Corripio (2003) presents a convincing way to deduce slope and aspect considering only four cells (see Figure 14, Equations 19 - 23). Moreover, in order to calculate slope and aspect, normal unit vectors are used. Based on this information, it was decided to calculate vectors normal to the surface using this method and add them into the normal VRM. These vectors were calculated as proposed by Corripio (2003), from there on the same methodology as suggested by Sappington and Veitinger was applied (see appendix for R-script).

$$a = (l, 0, \Delta z_a), with\ \Delta z_a = z_{i+1,j} - z_{i,j} \quad (19)$$

$$b = (0, l, \Delta z_b), with\ \Delta z_b = z_{i,j+1} - z_{i,j} \quad (20)$$

$$c = (-l, 0, \Delta z_c), with\ \Delta z_c = z_{i,j+1} + z_{i+1,j+1} \quad (21)$$

$$d = (0, -l, \Delta z_d), with\ \Delta z_d = z_{i+1,j} + z_{i+1,j+1} \quad (22)$$

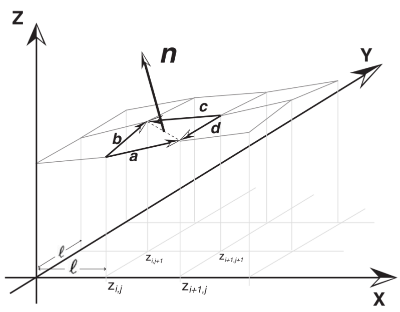

Figure 14. A different way to construct a normal vector considering only four points (Figure from Corripio 2003).

With these vectors a vector normal to the surface is constructed. A simplified form of the vector normal to the grid cell is denoted by:

$$n = \begin{pmatrix} \frac{1}{2} l(z_{i,j} - z_{i+1,j} + z_{i,j+1} - z_{i+1,j+1}) \\ \frac{1}{2} l(z_{i,j} + z_{i+1,j} - z_{i,j+1} - z_{i+1,j+1}) \\ l^2 \end{pmatrix} \tag{23}$$

In a second step, the normal vector has to be normalized to a unit vector in order to use the vector in the VRM. For this, first vector length $|n|$ is calculated from vector n with the components x, y, z. Vector length is then used to normalize each vector component (x_u, y_u, z_u).

$$|n| = \sqrt{x^2 + y^2 + z^2} \tag{24}$$

$$x_u = x/|n| \tag{25}$$

$$y_u = y/|n| \tag{26}$$

$$z_u = z/|n| \tag{27}$$

Having unit vectors, it is now possible to proceed normally for calculating the resultant vector by using the equation presented for VRM in order to calculate terrain roughness. This modified VRM measure will be referred for as CVRM in the following.

5.2 HS and SWE measurements

In order to address the research questions, HS and SWE had to be collected from different terrain surfaces at different time steps. This was done by measuring HS/SWE along a priori known transects using a GPR. Along these transects, manual measurements were also taken, to calibrate as well as to validate GPR-data. GPR-data had then to be post-processed in several steps until it was possible to extract HS/SWE.

5.2.1 Measurement setup

The basic idea was to capture snowmelt by repeated HS / SWE measurements at the same location during a sunny and meteorological stable period. As usual in snow hydrology, HS was measured in meters and SWE in mm. The data collection was performed, by dragging a GPR-sledge along predefined transects and validate and calibrate the GPR-data by manual measurements taken synchronously.

For the GPR-measurements, four shielded antenna pairs of type Mala Rd3 were mended into a two-part sledge shell (Figure 15). On the first sledge two antenna pairs with a frequency of 1300 MHZ and one antenna with a frequency of 400 MHZ were installed. On the back sledge three antennas with a frequency 400 MHZ were mounted. This made the second sledge slightly lighter. The antenna setup is further illustrated in Figure 15 and Table 1 and Table 2.

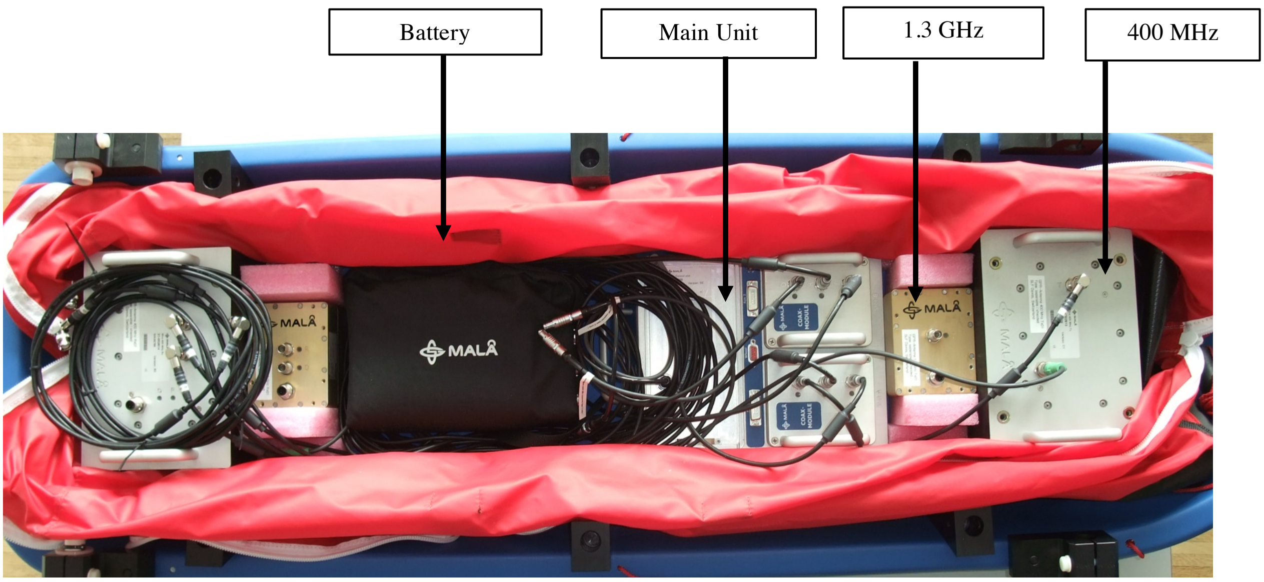

Figure 15. GPR setup of the front sledge (photographed by Tobias Jonas 2015).

Table 1. Antennae set up.

	Antenna 1	Antenna 2	Antenna 3	Antenna 4	Antenna 5	Antenna 6	Antenna 7	Antenna 8
Freq	1300MHz	400MHz	1300MHz	1300MHz	1300MHz	400MHZ	400MHz	400MHz
ID	RX2	TX2	TX2	RX1	TX1	RX2	RX1	TX1
Height above snow [m]	0.02	0.02	0.02	0.02	0.02	0.02	0.02	0.02

Table 2. Resulting antenna pair properties.

FILE	RX	TX	SEPARATION
A1	RX1	TX1	0.09
A2	RX1	TX2	0.32
B1	RX2	TX2	0.66
B2	RX2	TX1	1.07
C1	RX1	TX1	0.165
C2	RX1	TX2	2.23
D1	RX2	TX2	1.52
D2	RX2	TX1	0.875

Additionally to this setup, a hip chain was installed at the back of the second sledge. The hip chain is basically a small reel with a coiled thread. The end piece of the thread was then fixed to an anchor (e.g. a shovel put into the snow). When the sledge started to move along the transect, the distance of the measurement to the starting points could be traced by counting the times the reel was spinning. As an alternative to the hip chain, a small GPS was installed and directly connected to the GPR-measurements. Batteries were also installed on the sledge powered antennas and other equipment. On each side of the sled two ropes with handles were attached that allowed the sledge being pulled by two persons, one on each side. All measured data was put together and fed to a computer carried by one of the pullers.

This setup was then dragged along the previously defined transects. Along the transect markers were set every 20m -30m, both in the data using the board computer and visually with a flag in the field (see Figure 16). At each flag, HS and SWE were measured. For measuring HS, an avalanche probe was used. A measurement at the marker, as well 1m and 2m backwards were taken. For the SWE measurement, a federal SWE sampler was used. It is a tube with "teeth" that was pushed into the snow until it hit the ground. Ideally the underground would be a meadow so that the sampler can be pushed a bit into the ground. Then the sampler was turned in order to cut out the core. After it was taken out, traces of the soil at the bottom of the tube had to be removed and the sampler with the snow core was weighted. Knowing the weight, HS and the sampler diameter, Rho and SWE can be calculated. The problematic part is to use this kind of sampler when there is rocky underground or an ice layer. Then one cannot be sure whether the extracted snow core includes the complete snow column. At each transect also a snow pit was dug, in order to make reference measurements and liquid water contents (LWC) measurements. LWC measurements were done using a device built by the SLF workshop similar to a Denoth device. It takes half-space measurements. For every 10 cm the electric conductivity was measured and a SWE as well as a snow density sample was taken. With this, LWC of snow was calculated. Besides these measurements, snow height and SWE and snow density of the total snowpack were measured using a SWE sampler. This SWE sampling system proved to be in general more reliable, because one could see whether it hit the ground or not.

Figure 16. Measuring transect 7 at Monbiel. The GPR sledge is pulled by two people. The flag shows the location of a GPR marker, where also manual measurements were taken (photgraphed by Lucie Eberhard).

5.2.2 Measurement Campaigns

To apply the measurement approach described above, several requirements had to be met. First of all a precipitation free period close to the assumed POW of each fieldsite had to occur. During this time, also more practical reasons like staff and car availability determined the days on which the measurements were taken. Measurements had to be taken in the morning after cold, cloud free nights, since a snow crust was a requirement. With a snow crust, the persons pulling the sledge - as well as the sledge itself - would not sink in and alter the snow surface and hence the melting. Therefore measurements could not be taken at a fixed interval. The field days are described closer in Table 3. From experience from the snow hydrological group, it was decided that an interval shorter than two days would result in too small differences in HS / SWE. Initially two additional transects were planned for the survey at the Monbiel fieldsite. Because they were northerly exposed and thus snow ablation would start later, the first measurement was taken on the 19.03. Due to the heavy rainfalls and starting of campaigns at Sertig, it was not possible to measure this transect another time. For more information concerning air temperature and snow height changes see Figure 9 and 10.

Table 3. Overview Fieldwork, spring 2015.

Date	Time	Transect	Location	Time step
09.03.2015	09:18-10:02	1-5	Monbiel	T1
11.03.2015	08:36-09:40	6-7	Monbiel	T1
18.03.2015	07:21-10:28	1-7	Monbiel	T2
21.03.2015	06:48-08:53	1-7	Monbiel	T3
08.04.2015	05:50-09:07	1-4	Sertig	T1
13.04.2015	05:03-07:29	1-4	Sertig	T2
16.04.2015	05:10-06:37	1-4	Sertig	T3
21.04.2015	05:14-06:31	1-4	Sertig	T4
24.04.2015	06:51-08:45	1-4	Sertig	T5

5.2.3 Post-processing of GPR data

In order to be able to deduce HS and SWE from the GPR measurements the data had to be post-processed. In a first step data was processed with the software ReflexW. For this .rd3 data files from the Mala antennas were imported -. ReflexW creates a radargram (see Figure 17) from the measurements. For optical enhancement, the GPR raw data can be filtered. Most often a subtract DC-Shift was applied. Subtract DC-shift is a 1D-Filter that removes initial offset from the base guideline. Some transects were also filtered with the manual gain option. Manual gain (y) filter amplifies regions of interest of the radargram on the y-axis. The major step in ReflexW was then to define manually the upper and the lower boundary of the snow cover. In Figure 17 the blue arrow shows the direct wave (= snow surface), while the red arrow shows the bottom wave (= snow-soil interface). To mark the direct wave and the bottom wave, the option “pick – set” was chosen and the files were stored both as ReflexW file (for correction) as well as ASCII file (for further use in GPR4snow).

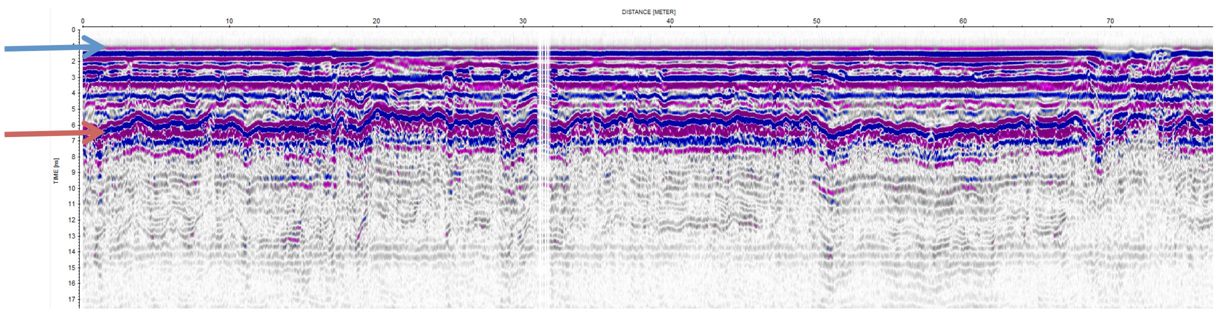

Figure 17. Radargram as shown using ReflexW. The blue arrow indicates the direct wave and the red arrow points to the bottom wave. When analyzing the radargram, the direct and the bottom wave hat to be identified first and then marked by with the picking tool. In that way, information about the direct and the bottom wave could be stored to further use it to analyse HS and SWE from the corresponding measurement location.

The .rd3 file (.asc) providing the measurements and the pick files (.asc) providing the snow boundaries as well as the manually collected data and antennas setup were then used to calculate SWE and HS. This was accomplished by using GPR4snow, a Matlab based program written by Tobias Jonas. In a first step, antennae setup and manual measurements were used to make a CMP analysis. In a second step, radar waves were transformed to HS, SWE or snow density. For the second step the user has different options at hand. Dry and wet snow can be distinguished. Since snowmelt was measured the wet snow option was taken. Further the analysis method can be chosen. Options are based on measurements only, reducing minimum error in RMSE, SWE, HS or combined HS/SWE options. To calculate SWE different equations calculating dielectric properties heterogeneous materials can be used such as the one proposed by Looyenga (1965), closer explained in 2.2.3. To give the program reasonable values to start calibrating radar data, average snow depth, density and LWC can be given.

Looking at the output for one transect from the different measurement campaigns it became evident that the trace numbers (the number of radar measurements) of each transect at the different timesteps varied somewhat. When plotting over each other, a slight shift could be observed. In order to see processes at the same locations the idea was to shift marker points that should be at the same location in every measurement campaign over each other. It was then decided that best solution was the synchronisation function of Matlab implemented in a Matlab script by Tobias Jonas. It shifts HS / ΔHS or SWE / ΔSWE together using marker locations. To lessen the scatter of the measurements a moving window option can be chosen. In an addition the goodness of fit between manual and radar measurement of HS or SWE can be obtained. For this first measurements at the markers from the different time steps were subtracted from the initial measurement. This was done for both manual and GPR measurements and then plotted against each other. This gives an idea of the performance of the GPR-measurements. Based on this assumption the root mean square error (RMSE) between GPR-measurement and manual measurement can be calculated. RMSE can be optimized by choosing different window sizes to calculate HS / SWE. Looking at the RMSE from the different transect also helped to compare the quality of measurement between the transects.

5.3 Data Analysis

After obtaining many data by calculating HS, SWE and terrain roughness a first overview of further analysing steps was made.

5.3.1 Basic data analysis

First the two roughness measures were compared to each other and evaluated. For this the final roughness map was compared to ground reality. To compare the two roughness measures better, they were both normalized since maxima and minima were slightly different. To compare VRM and CVRM better following equation (Grohmann et al. 2011) was applied to standardize both values:

$$\frac{(\text{map value} - \text{map min})}{(\text{map max} - \text{map min})} \tag{28}$$

Also histograms were created in order to compare the variability of terrain roughness at the two sites (see Figure 20).

For the measurement data, HS and SWE variability of the different measurement days were looked at and compared to the manual measurements. This was done using the Matlab scripts mentioned in 5.2.3. With those scripts, also RMSE between the manual measurements and the GPR measurements was calculated.

In order to compare the different fieldsites and transects to each other basic descriptive (min, max, mean, SD, C_v, variation and total ΔSWE) were calculated. Furthermore, two histograms were made to illustrate the variation of HS and SWE at POW.

5.3.2 Hysteresis Approach

Taking the scenario of homogenous melt rate, the relationship between SD of HS and mean of HS was

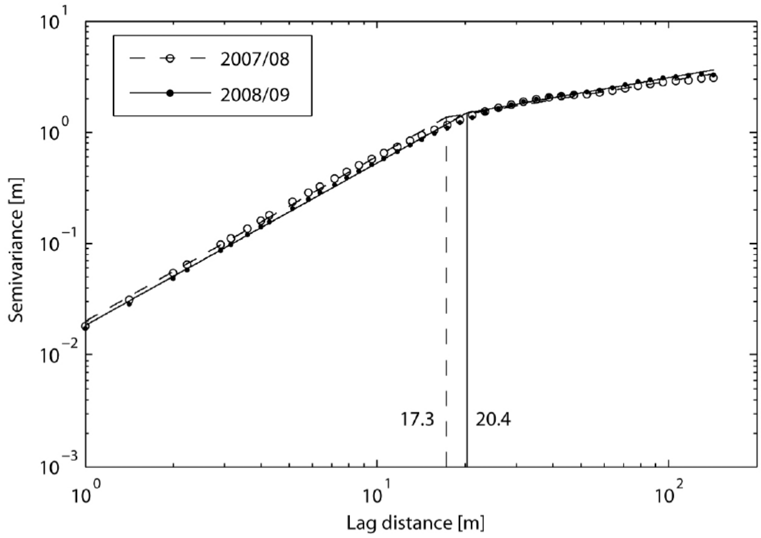

Figure 18. Variogram showing the semivariance of a crossloaded slope (Figure from Schirmer & Lehning 2011)

investigated. This analysis is based on the hysteresis approach as first proposed by Egli & Jonas (2007). Transects and their corresponding measurements were divided into 20m long slices. 20m was chosen, because Schirmer and Lehning (2011) found a scale break at approximately 20m. A scale break with a variogram means that data on the right side of the scale break has hardly any autocorrelation, whereas data with a scale smaller than 20m (on the left side) show more potential autocorrelation. Data from each 20m slice was averaged so that each 20m slice became one HS / SWE measurement. With those new data points mean and SD was calculated for each of the two field sites. This was done for all interals. In plotting them together the coefficient of variation is shown. Aim is to be able to compare this to similar plots shown by Egli et al. (2011).

5.3.3 Snow Ablation and Terrain Roughness

Firstly, summer terrain was directly compared to winter terrain at the measurement intervals during snow melt. For this HS / SWE was added to elevation in order to create the elevation of winter terrain. SWE values had to be first transformed to meters. Summer as well as winter terrain were then separately detrended (linear detrend). For both, summer terrain (detrended elevation) and winter terrain (detrended elevation + HS/SWE from different time steps), SD was calculated.

To see whether there was a variation between either depletion at the measurement intervals or between different transects the ratio of the two melting rates was looked at.

In a second step HS and SWE at POW, as well as different melting periods were plotted against terrain roughness (CVRM). This was done to see whether there is a correlation between HS and SWE and terrain roughness. In case terrain roughness was averaged out too much by the 20m approach, also raw measurement data was plotted against the corresponding roughness.

6 Results

6.1 Basic Results

In this chapter the preliminary results will be presented. First the results of the terrain roughness analysis will be looked at and discussed shortly. This is done for the reason that terrain roughness at the different transects is used as a dataset for further analysis. This subchapter will be followed by a presentation of the measured HS and SWE data to give an oversight over the dataset at hand.

6.1.1 Terrain Roughness

Comparing the two terrain roughness measures VRM and CVRM, they yield very similar results over all.

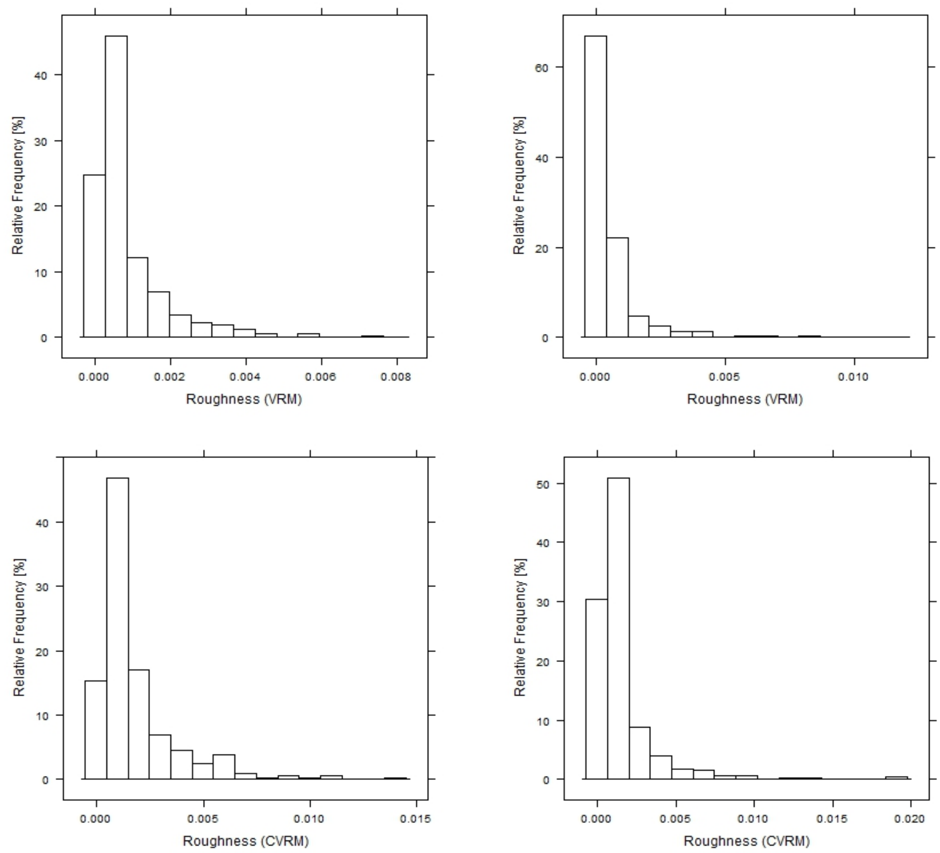

Figure 19. Histogram of both VRM (top) and CVRM (bottom) at Monbiel (left) and Sertig (right).

Both methods show similar features. Especially ridges are shown very distinct. It becomes clear that even though transects are not entirely smooth, they still have a rather low roughness compared to e.g. the rock faces and ridge at higher elevations. Analysing VRM and CVRM further, it is observable that the main differences are spotted when focusing on smoother terrain (see Figures 20 – 24). Where VRM shows a smooth area CVRM tends to illustrate minor differences in terrain. However when looking at the histogram from the two fieldsites of the two method they have a very similar shape.

Nevertheless, it was decided to use CVRM for its ability to show finer roughness variations for summer terrain than the VRM.

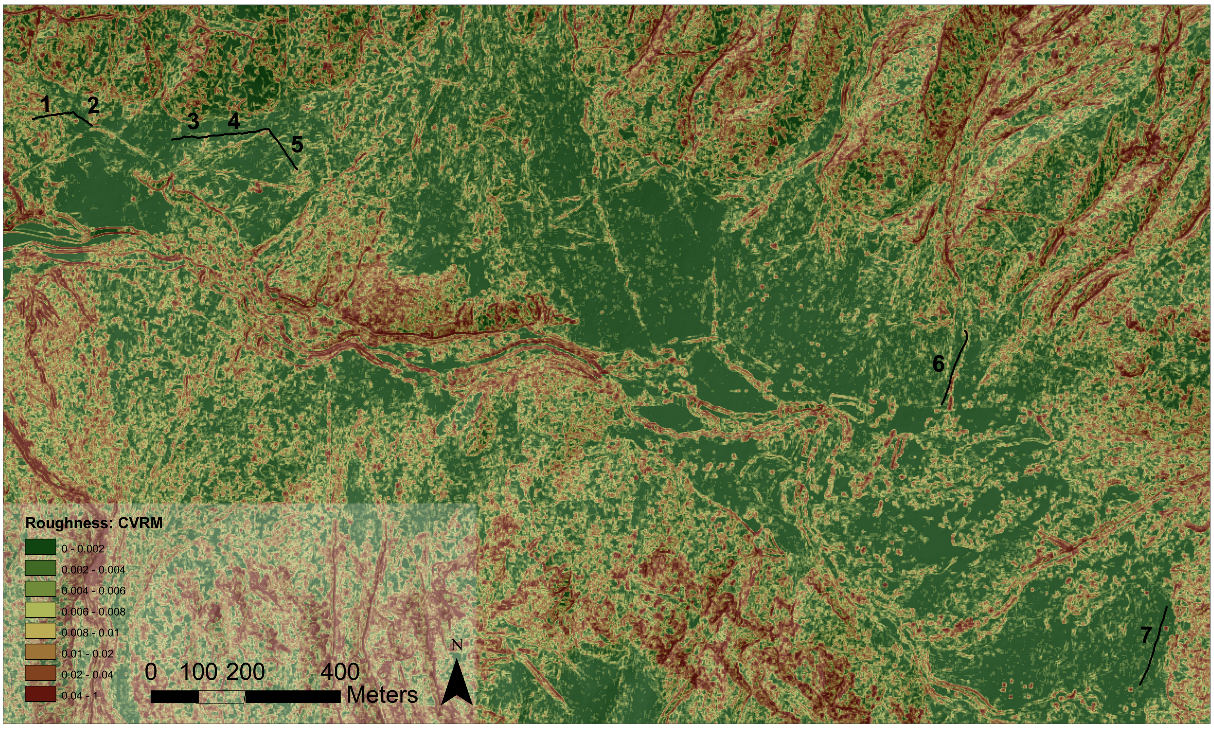

Figure 20. Roughness map of Monbiel using CVRM. Even small roughness changes are visible.

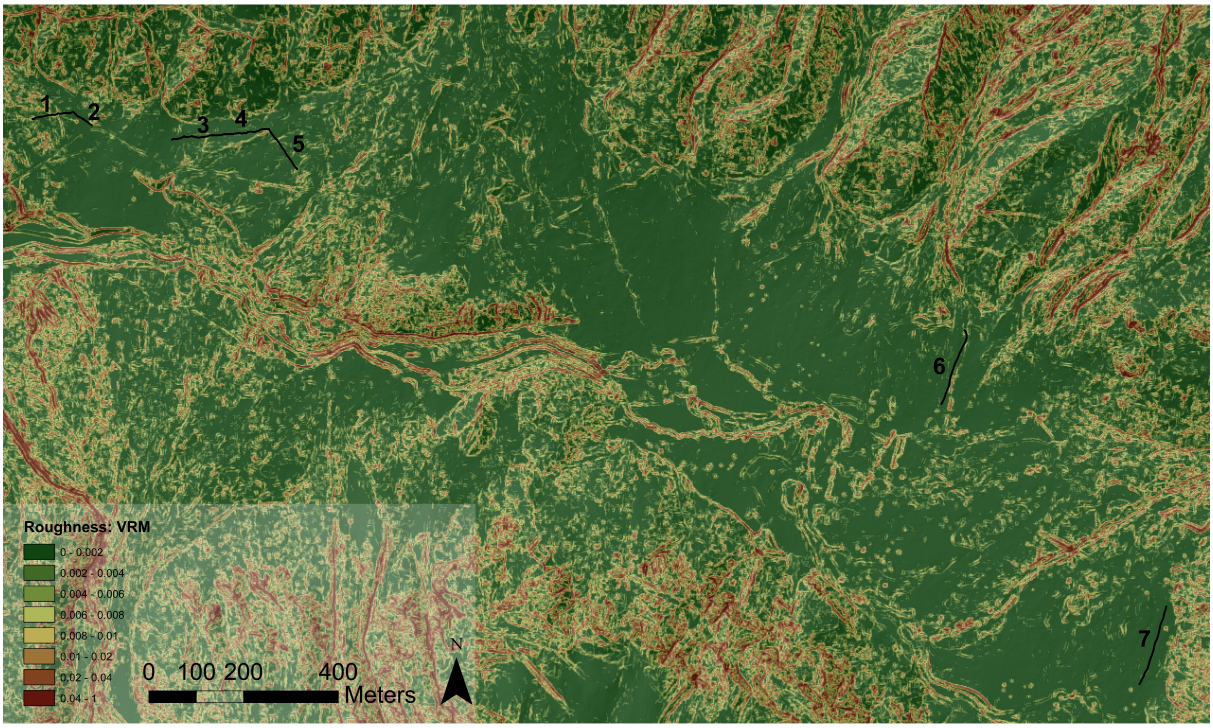

Figure 21. Roughness map of Monbiel using VRM. Rough terrain is depicted correctly, but does not show very small roughness changes.

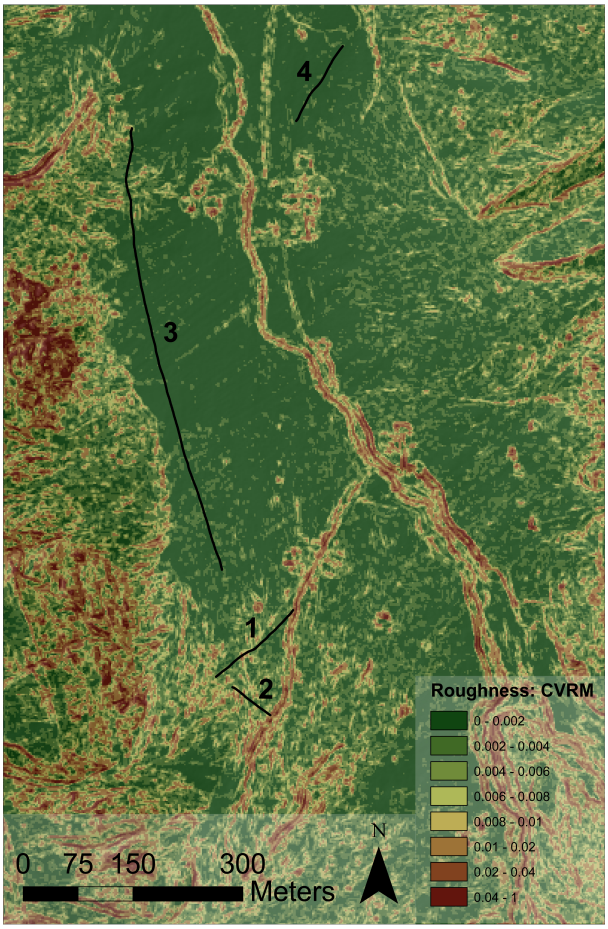

Figure 22. Roughness map of Sertig using CVRM.

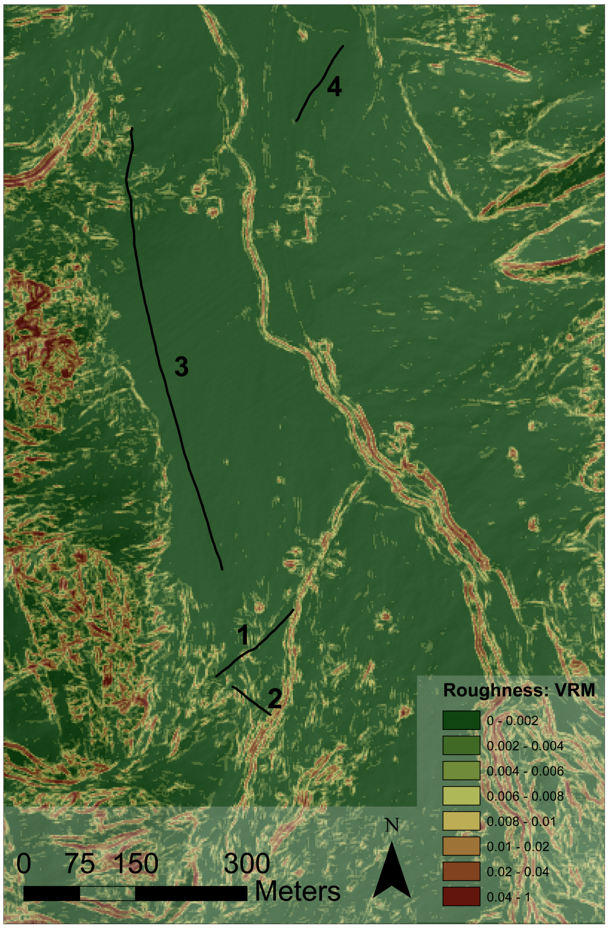

Figure 23. Roughness map of Sertig using VRM.

6.1.2 Resulting HS and SWE values

As a next step the characteristics final HS and SWE GPR measurements are presented. Those measurements build up the fundamental data, on which the further analysis is based. In the end of this part the method used to collect HS and SWE data is reviewed shortly. This is done in order to have a base to proceed to a more profound data analysis.

When analysing HS and SWE values the calculated RMSE between manual and GPR measurements played a crucial role. First, by optimizing RMSE value, the most efficient window size to calculate GPR measured HS and SWE values were determined. On average a window size of 14 yielded the best results for HS and SWE. Therefore the HS and SWE data that was used for further analysis was received using a window size of 14. When changing the number of transects taken into the RMSE calculation it was discovered that the goodness of RMSE was highly dependent on transects chosen. It especially made a difference, when in- and excluding S3.

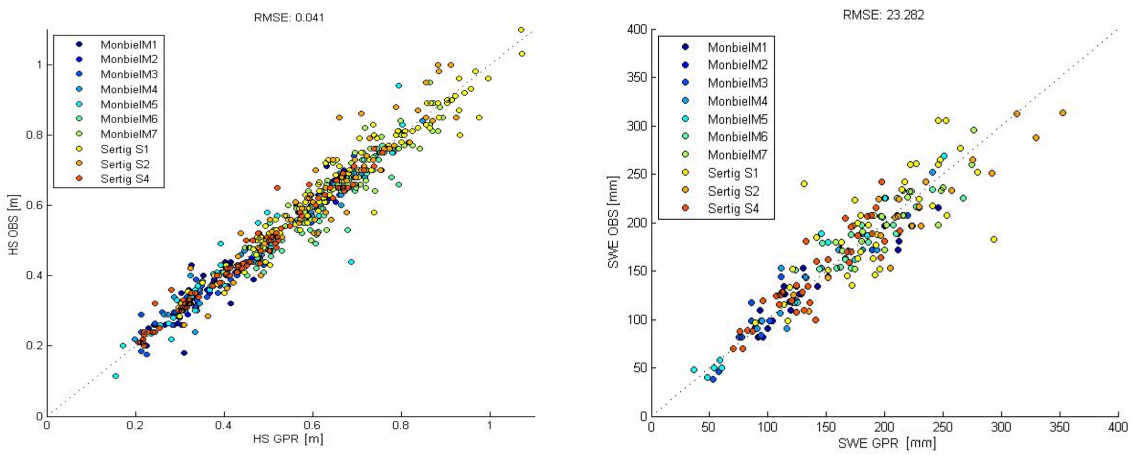

Figure 24. RMSE of GPR measurements without using S3. The left plot shows RMSE of HS and the right plot RMSE of SWE.

In Figure 24 RMSE is shown for all transects but S3. The RMSE for HS was 0.041m and for SWE 23.282mm. However when including S3 into the RMSE calculation, the RMSE of HS increased to 0.06m and the RMSE of SWE to 35.45mm. This seemed to be a lot to be explained only by measuring GPR inaccuracies. Therefore S3 was investigated closer to find reasons for this. One thing that met the eye was that also manual SWE measurements were partly rather unrealistic. For example showed some measurements taken during a later campaign higher SWE values than in the campaign before. This was on the flat part before transect S3 gets rougher. Already during measurements it was suspected that there might be an ice layer. When snow fell out of the measurement tube due to the ice layer this explained the manual part of the measurement and thus unreliable calibration and validation values for the GPR measurements. But also when only considering GPR measurements some disagreement was found. Having a look at the radargram it is noticed that instead of being continuous, the lines, indicating measured underground boundaries, are often shifted. This phenomenon was in this multitude only observed at S3. It could be explained when considering the hip chain. Normal transects are more likely to be straight and therefore the hip chain that is always a direct line between the GPR and the starting point behaves in a very usable way. With S3 being by far longer than the rest of transects (ca. 600m instead of +/- 100m) it is plausible that here the hip chain did not work that well. Due to its unique length, the shape of the transect shows a slight curve. It is thus plausible that the hip chain started following the GPR’s track, held in place by the friction of the snow. When the tension on the hip chain got bigger (due to the longer way it was taking) it jumped back to minimal distance from time to time. Each time the hip chain jumped back there were few moments when the GPR did not measures, since the unwinding of the hipchain triggers the GPR to start measuring. A usually being a straight line to the starting point was jumped back from time to time to the minimal distance. Balancing those reason it was finally decided not to include S3 in any further analysis of HS and SWE from 6.2 onwards.

In Figure 25 the synchronized and final HS and SWE measurements along transect M4 are shown. The different lines show the different measurement days, the dots show the corresponding value of the manual measurements. For visual analysis one plot for each transect was created (see appendix). For Sertig the measurement differences from one measurement campaign to the next was in general rather low. It was therefore decided to only use the first (08.04.), the medium (16.04.) and the last (24.04.) measurement to visualize HS / SWE as profiles for the Sertig transects. The same dates were also used for differential analysis (see 6.3).

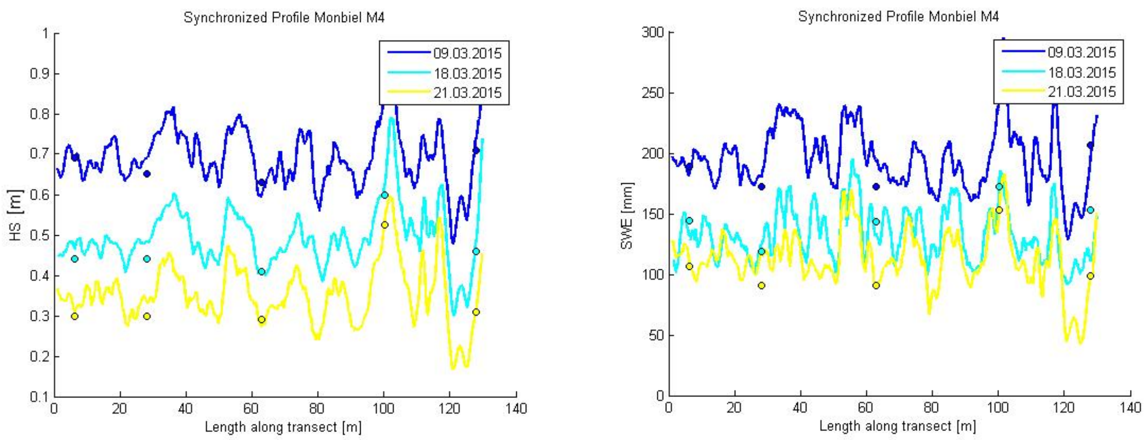

Figure 25. Synchronized HS and SWE profile for transect M4. The GPR measurements are shown as lines, manual measurements as points. The plots from the rest of the transects can be found in the appendix.

In Table 4 and Figure 26 a basic evaluation of HS at POW is shown. ΔHS is referring to the total snow depletion between the first and the last measurement. In general Sertig shows a slightly higher HS. The C_v is for both fieldsites similar. In Monbiel there were more measurements taken. Also Monbiel has a lower RMSE than Sertig. As already shown for RMSE of all transects S3 increases RMSE a lot. The RMSE of measured Sertig HS decreases from 0.073 to 0.042 when S3 is not included.

Table 4. Descriptive statistics of HS Measurement:. Mean, sd deviation, maximum, minimum, variance, cv HS refer to HS at POW. For the RMSE all calculated GPR values (moving window = 14) where compared to manual measurements at markers. ΔHS calculated by taking mean HS from POW and subtracting mean HS from the last measurement.

	Monbiel	M1	M2	M3	M4	M5	M6	M7	**Sertig**	S1	S2	S3	S4
Mean HS [m]	**0.65**	0.59	0.64	0.64	0.69	0.67	0.72	0.55	**0.81**	0.92	0.85	0.80	0.68
SD HS [m]	**0.09**	0.04	0.02	0.05	0.07	0.09	0.04	0.08	**0.10**	0.10	0.07	0.04	0.07
Max. HS [m]	**0.92**	0.67	0.69	0.73	0.92	0.84	0.84	0.67	**1.23**	1.23	1.01	0.92	0.93
Min. HS [m]	**0.30**	0.45	0.59	0.51	0.48	0.41	0.62	0.30	**0.52**	0.72	0.62	0.70	0.52
C_v HS [m]	**0.13**	0.07	0.04	0.07	0.10	0.13	0.06	0.14	**0.13**	0.11	0.08	0.05	0.11
Count	**14686**	1775	897	1529	2578	2066	3270	2571	**1225**	2718	1262	5977	2302
RMSE HS [m]	**0.04**	0.036	0.021	0.03	0.031	0.054	0.046	0.044	**0.073**	0.04	0.06	0.112	0.025
ΔHS [m]	**0.17**	0.22	0.24	0.20	0.20	0.24	0.07	0.18	**0.34**	0.39	0.30	0.33	0.34

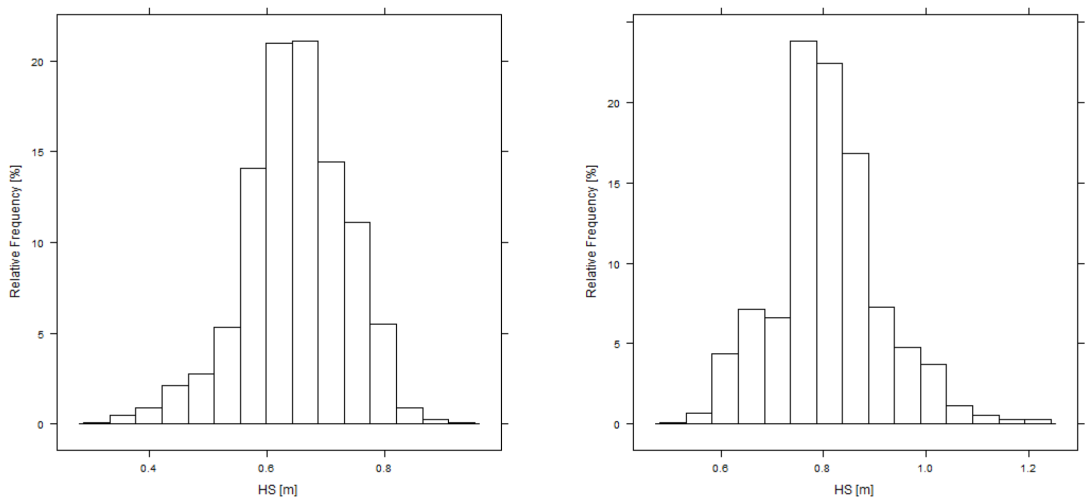

Figure 26. Histogram showing initial HS measurements taken at Monbiel (left) and Sertig (right).

Looking at SWE data mean values are in a similar ratio between Monbiel and Sertig than observed before with HS (see Figure 27, Table 5). SD and C_v are though relatively higher for Sertig than the used to be for HS. Looking at the RMSE there is again a major difference when including S3 or not. RMSE of SWE at Sertig decreases from 45.48 to 29.47.

Table 5. Descriptive statistics of HS Measurement: Mean, sd deviation, maximum, minimum, variance, cv SWE refer to SWE at POW. For the RMSE all calculated GPR values (moving window = 14) where compared to manual measurements at markers. ΔSWE calculated by taking mean HS from POW and subtracting mean SWE from the last measurement.

	Monbiel	M1	M2	M3	M4	M5	M6	M7	**Sertig**	S1	S2	S3	S4
Mean [mm]	**205.80**	211.24	180.23	191.55	194.81	189.17	232.75	211.24	**228.83**	255.37	324.68	207.32	200.80
SD [mm]	**30.01**	24.18	13.95	16.80	25.57	28.45	26.00	24.18	**52.21**	51.46	28.38	30.37	26.42
Max. [mm]	**299.76**	254.35	215.99	229.33	295.37	261.99	299.76	254.35	**395.74**	395.74	388.88	298.55	325.21
Min. [mm]	**120.98**	142.96	156.90	156.65	128.28	120.98	164.62	142.96	**135.47**	145.60	240.88	135.47	164.33
C_v [mm]	**0.15**	0.11	0.08	0.09	0.13	0.15	0.11	0.11	**0.23**	0.20	0.87	0.15	0.13
count	**13890**	1775	897	1529	2578	2066	3270	1775	**12259**	2718	1262	5977	2302
RMSE SWE [m]	**16.59**	17.33	7.03	15.79	15.54	17.69	17.57	17.88	**45.48**	37.87	25.52	66.84	20.35
ΔSWE [mm]	**70.75**	101.25	54.13	87.57	62.59	51.06	53.31	101.25	**77.55**	105.26	99.48	58.16	82.73

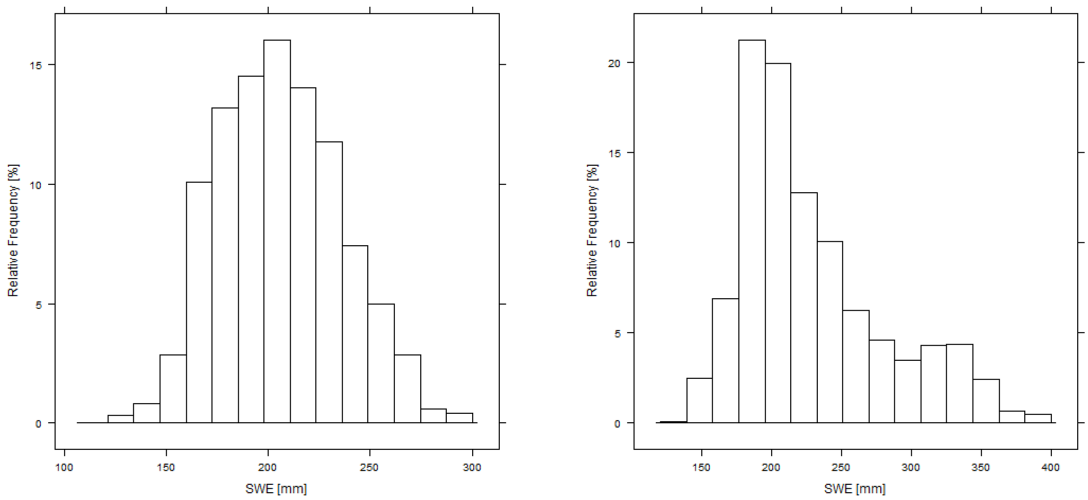

Figure 27. Histogram showing initial SWE measurements taken at Monbiel (left) and Sertig (right).

6.1.3 Evaluation on using GPR for snow measurements

To be able to focus further only on the actual application of the GPR data, the quality of the assessed data as well as the measurement set up will be discussed early.

Considering the RMSE of both HS and SWE, it can be stated that measurements by GPR is comparable in terms of accuracy to other remote measuring systems e.g. terrestrial LiDAR scanning (Bühler et al. 2015). It is theoretically possible to derive differently ΔHS and ΔSWE directly for the measured data for each time step. Since the snow depletion / snowmelt between certain timesteps was smaller than the RMSE, the main focus was placed upon the absolute measurements. At Sertig the differences of SWE between two measurement campaigns were just around the RMSE. To avoid RMSE to be bigger than the difference in HS / SWE only two melt time steps instead of four. This may seem like a waste of fieldwork, it however proved to be crucial to take measurements in this frequency in order to be able to see the GPR tracks from the previous measurements. Knowing where the GPR track was from the previous campaign was essential to ensure that the same path was taken twice. It is also wise to have more measurement campaigns than less in case of a malfunctioning of the GPR.

The explicit advantage over manual measurements is the high density of measurements that can be acquired at a very short time. Even though measurements were smoothed / averaged in post processing it gives a very distinct overview over snow cover variability that is not biased by preferential manual measurements. Comparing GPR-measurements to LiDAR scanning, digital photogrammetry or other

Figure 28. Advanced snow melt at Sertig valley. The two photographs show transect S3 at Sertig. The left pictures shows the view to the south (valley end) and the picture right faces north (valley opening, Frauenkirch). Keeping to the original track was difficult to impossible at such locations.

remote measuring systems it has the clear disadvantage of providing only 1d data when using our measuring approach. Due to measurement strategy melting out of snow cannot be measured, since the sledge cannot be pulled over snow free space, especially if there are some rocks there. During the final measurement campaigns this problem was encountered at M1 and S3, both rather rough transect where it would have been interesting to see, how snow melts out. This leads to a limited overview over the whole area. However, the ability to measure SWE directly (apart from using manual measurements for calibration), is in clear advantage since it does not rely on a statistical relationship between snow density and HS that is needed to calculate SWE from many HS measurements and occasional snow density / SWE measurements.

This ability grows in importance when very accurate SWE values have to be obtained of an area. Looking for example at Figure 35 it is shown here very nicely that ΔHS can indeed vary from ΔSWE. If ΔHS of M7 is compared to ΔHS of M6 they both show an average snow depletion of approximately 0.2m. Considering ΔSWE however, snow at M6 has melted about 100mm whereas snow at M7 only melted about 20mm. This is even more striking since M6 and M7 are rather close to each other and show a very similar exposition and elevation. Considering the location in the valley, M7 is closer to the foothill of a nearby mountain (Canardhorn), while M6 lays on a open surface.

6.2 Hysteresis Approach with GPR Measurements

As described in 5.3.2, it was attempted to reproduce the hysteresis approach as first presented by Egli & Jonas (2009) and complement it with SWE measurements. In the following the results of this analysis will be presented.

Table 6. Mean, SD and corresponding C_v from the two fieldsites for HS and SWE. For row "Overall" C_v was calculated from the average of Mean / SD of the corresponding fieldsite. T1-T5 indicate the different measurement times. It should be mentioned that Tx of Sertig is not equal with Tx of Monbiel.

	Monbiel						Sertig					
	HS			SWE			HS			SWE		
	Mean [m]	SD [m]	C_v	Mean [mm]	SD [mm]	C_v	Mean [m]	SD [m]	C_v	Mean [mm]	SD [mm]	C_v
Overall	**0.56**	**0.12**	**0.2**	**164**	**41**	**0.25**	**0.58**	**0.12**	**0.21**	**182**	**43**	**0.24**
T1	0.71	0.09	0.13	211	23	0.11	0.82	0.13	0.16	248	50	0.20
T2	0.54	0.13	0.24	155	42	0.27	0.67	0.12	0.18	205	31	0.15
T3	0.44	0.15	0.34	127	59	0.46	0.56	0.11	0.20	184	51	0.28
T4							0.46	0.12	0.26	152	43	0.28
T5							0.38	0.13	0.34	120	39	0.33

Table 6 shows the mean and SD for HS and SWE at the two fieldsites. By dividing SD with mean C_v was obtained. In Figure 29 this relationship is shown graphically. Looking at the left side of Figure 30 the ratio for SD HS and mean HS is shown. Monbiel shows a decreasing mean HS (from 0.7m to 0.44m) while SD HS increases from 0.09m up to 0.15m. Although mean HS decreases for Sertig too (from 0.8m to 0.37m), SD HS stays around 0.12m. Looking at the right side of Figure 30 there is a similar trend noticeable. For Monbiel mean SWE decreases from 211mm to 127mm, while SD SWE increases from 23mm to 59mm. Also at Sertig a similar observation to HS can be made: Mean SWE decreases from 248mm to 120mm. SD SWE shows appart from one outlier a relatively linear path from 50mm to 39mm. Comparing C_v of the timesteps HS and SWE the yield similar results. Looking at the total C_v of HS and SWE at the two fieldsites the values are nearly identical.

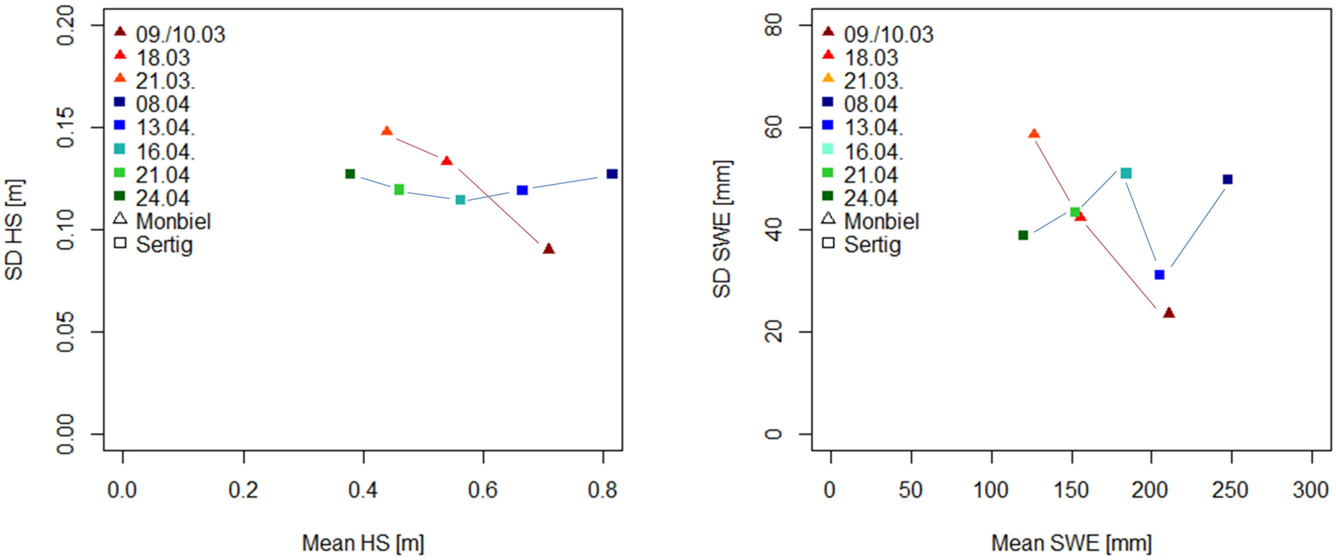

Figure 29. Development of the ratio between SD of HS and mean HS (left) and the ratio between SD of SWE and mean SWE.

6.3 Comparing Snow Cover to Terrain

In a second step it was analysed how terrain relates to different snow cover and snow ablation characteristics. Firstly, the correlation between C_v of HS and SWE was compared to terrain roughness.

6.3.1 Terrain Roughness and C_v

Considering the fact that HS and SWE have a greater variability in rough terrain this should also become visible with the measured HS and SWE data and the roughness measure. For every slice of each transect Mean and SD was calculated. By dividing SD by the mean C_v was obtained. C_v of HS as well as SWE was then plotted against CVRM.

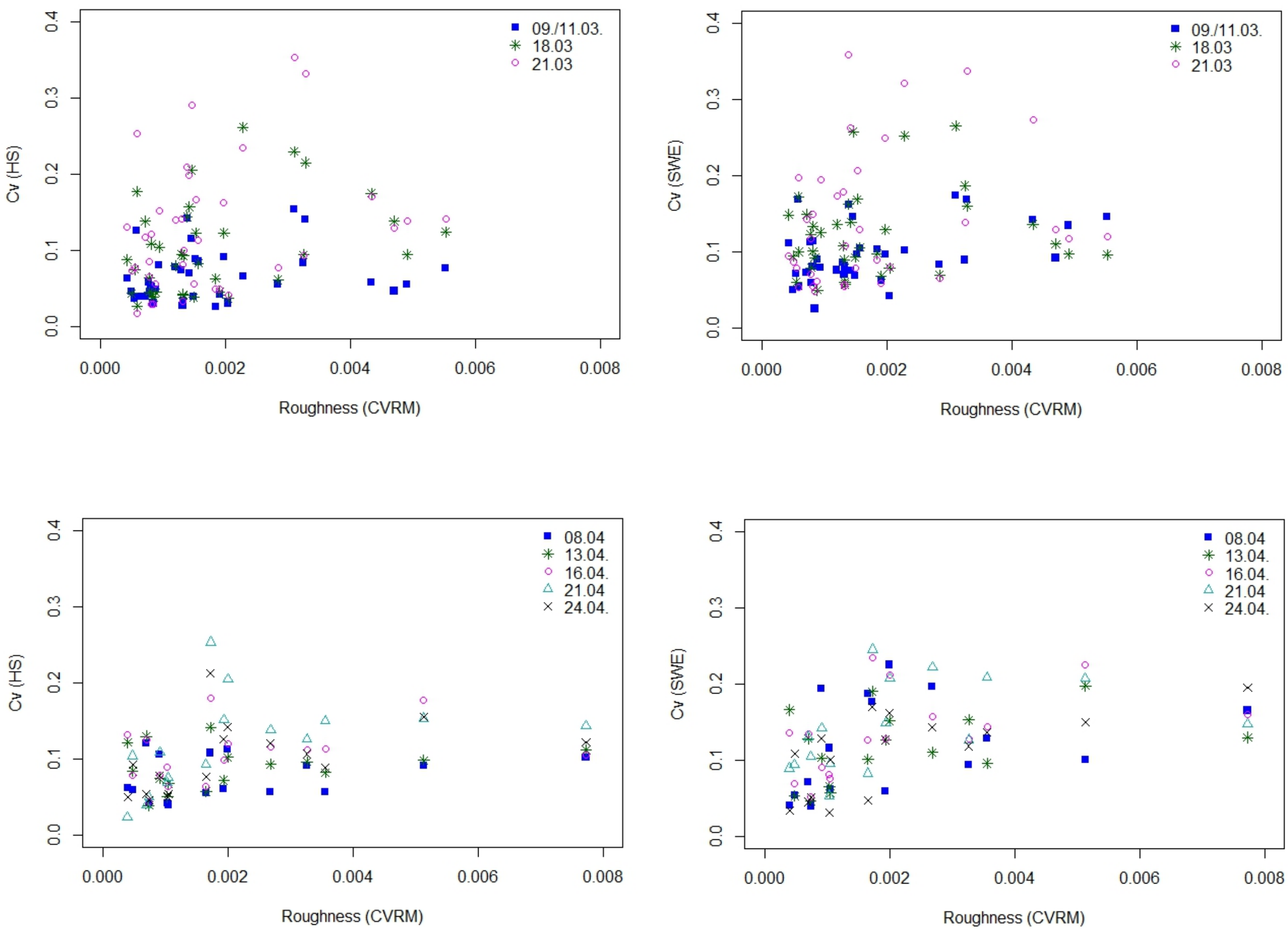

Figure 30. Relationship between C_v and terrain roughness (CVRM) for HS (left side) as well as SWE (right side). The two plots at the top show the results for Monbiel and the two plots below show results for Sertig.

Looking at Figure 31 there is some sort of relationship. Especially C_v of SWE shows a certain correlation. To have confirmation from the statistical side it was decided to perform a Spearman Rang Correlation test, due to the fact that CVRM proved to be not normally distributed. As null hypothesis (H_0)

there is no correlation assumed while for the alternative hypothesis (H_1) there is a correlation assumed. Significance level lies at 0.05. R is the correlation coefficient that shows the degree of correlation, with having (-) 1 as perfect (anti-) correlation and 0 as no correlation.

Table 7. Correlation between C_v of HS / SWE at different time steps and terrain roughness (CVRM). A Spearman Rang Correlation was performed, with r = correlation coefficient and significance level at 0.05. T1 – T5 indicates the time steps again.

	Monbiel				Sertig			
	HS		SWE		HS		SWE	
	p-value	r	p-value	r	p-value	r	p-value	r
T1	0.12225	0.26	0.0216	0.38	0.6407	0.13	0.0517	0.49
T2	0.36	0.279	0.4082	0.14	0.5717	0.15	0.137	0.39
T3	0.32	0.516	0.0457	0.33	0.3108	0.27	0.0108	0.62
T4					0.00009	0.75	0.0094	0.63
T5					0.003	s	0.0011	0.74

The statistical values in Table 7 show that for SWE the majority of time steps show a weak to real correlation of C_v of SWE and CVRM. Surprisingly there is less evidence so for C_v of HS though: Only T4 and T5 of Sertig show a provable correlation. The other values have partly a quite high coefficient of variation but that cannot be proved statistically.

6.3.2 Connecting Measurements to Terrain and Assessing Snow Melt Rates

Figure 33 shows the relationship between the SD of elevation of summer terrain and SD of elevation of winter terrain. SD of elevation can also be looked at as a roughness measure. The left side of Figure 33 shows the result for HS measurements and the ride side for SWE measurements. Both plots show a relatively small variation and group close to the y=x line. There is no recurring pattern visible.

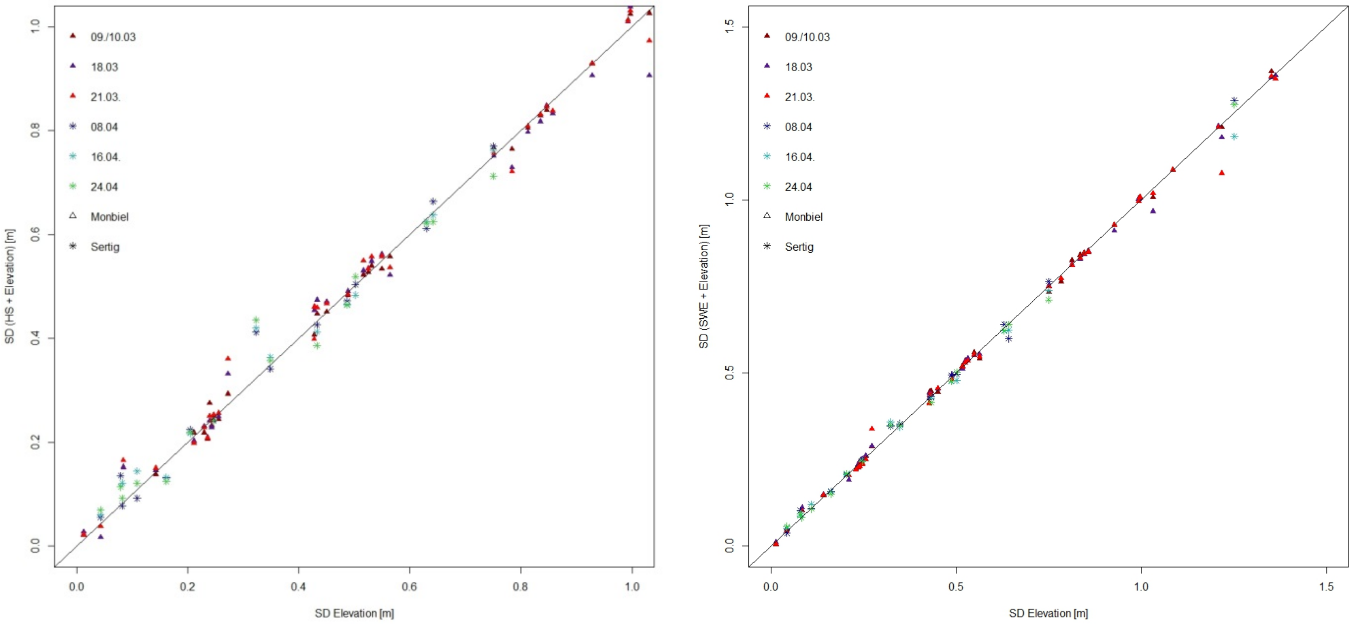

Figure 32. SD of HS / SWE at different timesteps plotted against SD of elevation. For this case, SD of HS / SD of SWE were calculated by adding HS / SWE measurement to the corresponding elevation. Therefore SWE values had to be transformed from mm to m first.

For the next step snow ablation was looked with a differential approach. For this HS / SWE of different dates were subtracted. In Table 8 three different snow ablation rates are defined.

Table 8. Overview over defined snow ablation rates.

Fieldsite	ΔHS/ ΔSWE	ΔHS1/ ΔSWE1	ΔHS2/ ΔSWE2
Monbiel	09./11.03. – 21.03.2015	09./11.03. – 18.03.2015	18.03. – 21.03.2015
Sertig	08.04. – 24.04.2015	08.04. – 16.04.2015	16.04. – 24.04.2015

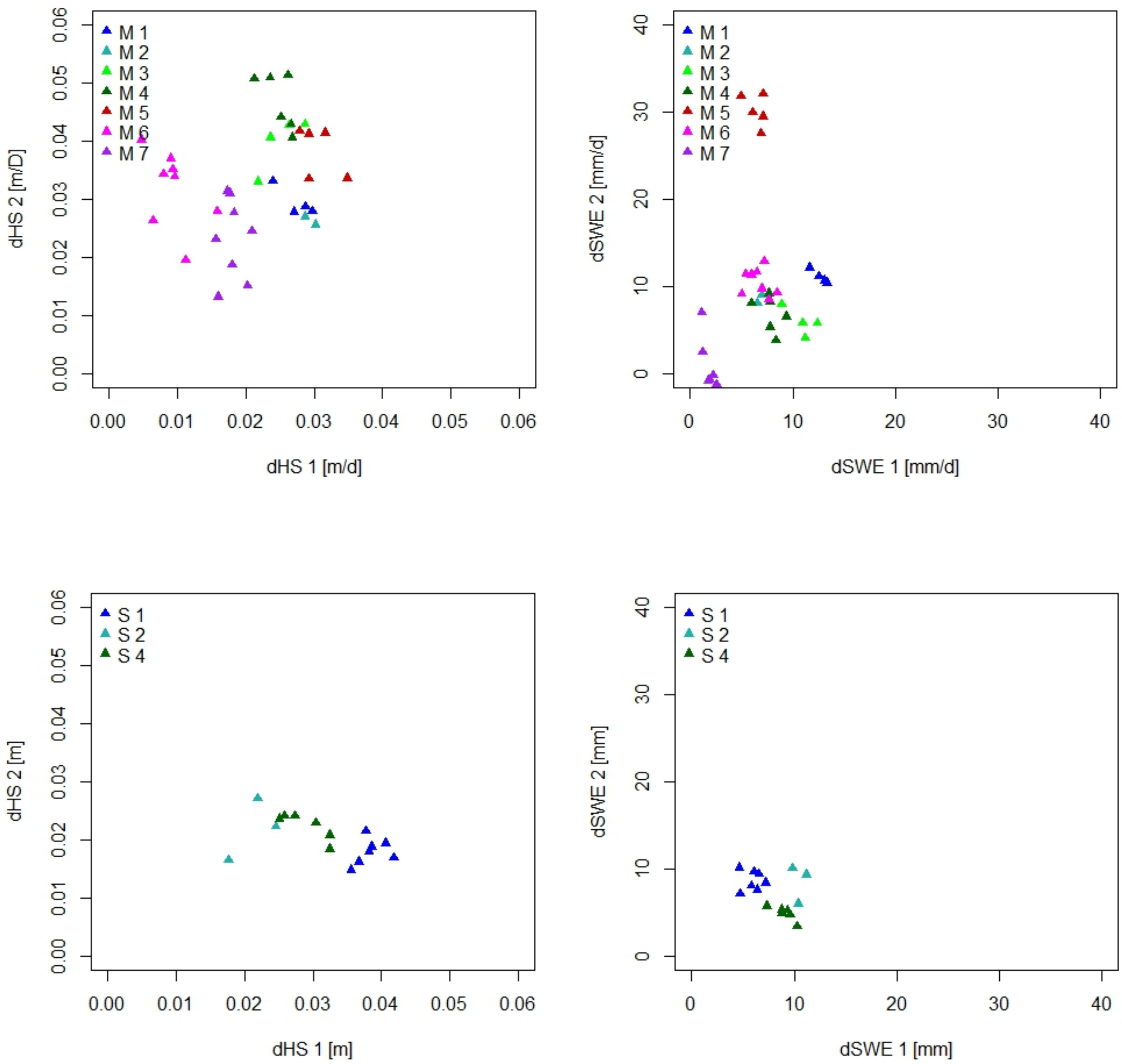

Figure 33. Ratio between ΔHS1/ΔSWE1 and ΔHS2/ΔSWE2 for both Monbiel (top) and Sertig (bottom). Colors show the different transects.

First melt rates of the 2 measurement intervals of each fieldsite were calculated. In a second step ΔHS1/ ΔSWE1 were plotted against ΔHS2/ ΔSWE2 in Figure 34. The two plots at the top show this ratio for Monbiel, the lower two for Sertig. ΔHS are in general slightly lower for Sertig than for Monbiel. ΔSWE however yields very similar results. At Monbiel it is observable that between transect there was different melt. For example shows transect M7 less snow depletion and snowmelt than transect M1. At Sertig ΔHS1 is higher than ΔHS2, even though having a similar amount of days between the two melting periods. Although for ΔSWE1 and ΔSWE2 this pattern cannot be seen.

6.3.3 Relationship between Snow Ablation and Terrain

In a further step HS and ΔHS (left) at POW as well as SWE and ΔSWE (right) at POW were plotted against CVRM (Figure 35).

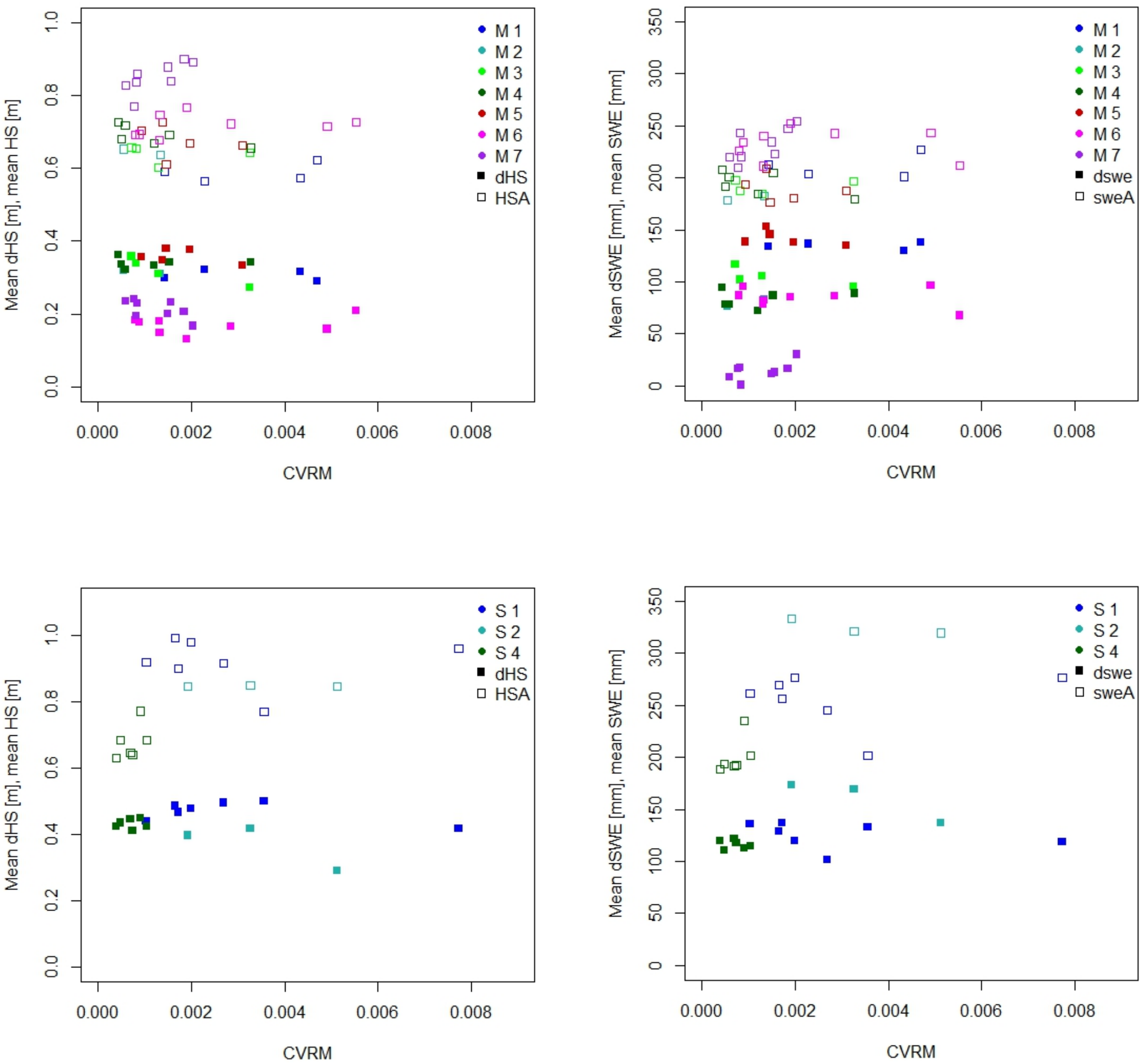

Figure 34. HS/SWE at POW and ΔHS/ΔSWE plotted against CVRM. Plots for Monbiel are at the top, plots for Sertig at the bottom. Mean HS denotes mean HS within the slices at the first measurement date.

Both figures do not reveal a special spatial trend. It is though observed that some transect show relative to the other transects a different pattern for ΔHS than ΔSWE. For example have transects M6 and M7 a very similar ΔHS, while they differ when looking at ΔSWE. Also HS/SWE patterns are different than ΔHS/ΔSWE patterns. For example are the measurements of M4 and M5 for SWE located very closely together at peak of winter when they do not for ΔSWE. Neither ΔHS/ΔSWE nor HS/SWE show any specific correlation to terrain roughness.

To further investigate this issue the relationship between ΔHS/ΔSWE or HS/SWE and aspect / slope were looked at. The results (Figure 36) showed that there is a correlation between ΔHS/ΔSWE at Monbiel and slope. The correlation is also proved statistically and yields a correlation coefficient of r = 0.65 for ΔHS and slope at Monbiel, whereas for ΔSWE and slope at Monbiel r = 0.68. For Sertig no such correlation was found.

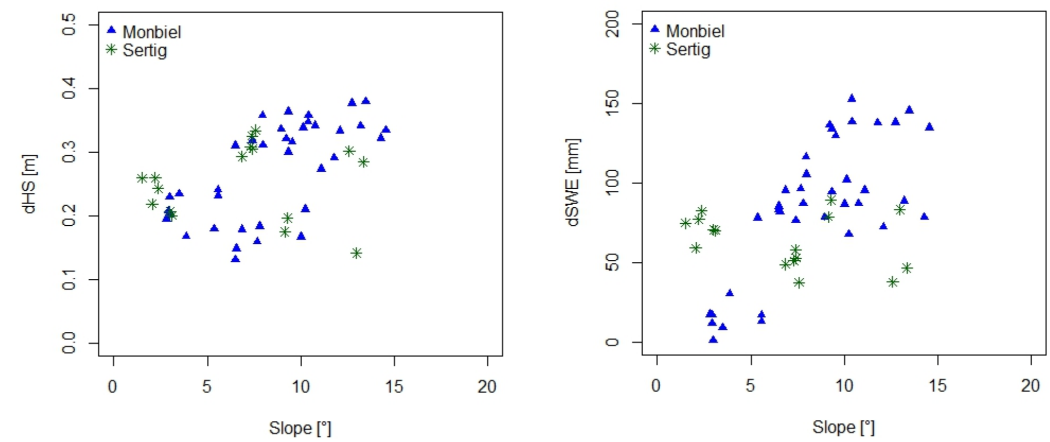

Figure 35. Relationship for ΔHS (left) /ΔSWE (right) and slope for Sertig and Monbiel.

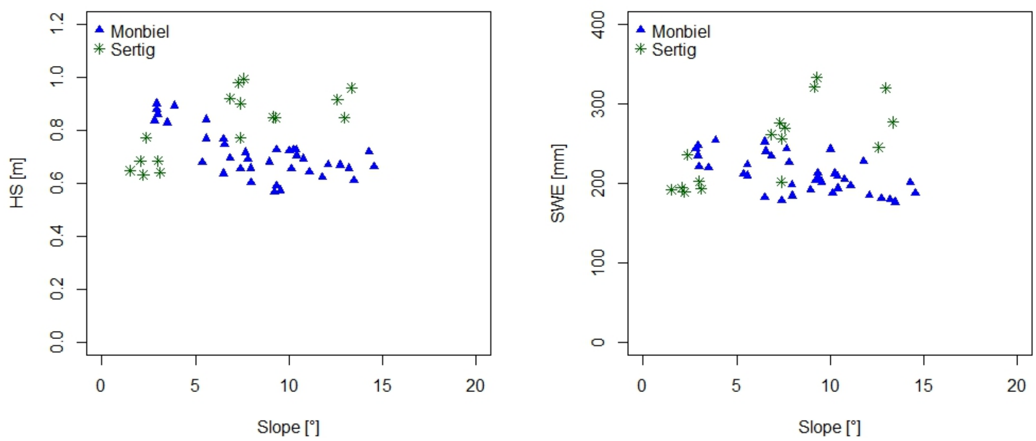

Figure 36. Relationshipbetween HS / SWE at POW and slope

When initial HS and SWE are plotted against slope (Figure 37) Monbiel shows for both HS and SWE an anti-correlation. The correlation coefficient for HS is r = -0.58 and for SWE r = -0.61. Both values show an anti-correlation, even though it is not very strong. Interestingly, Sertig shows a positive correlation with C_v for HS being r = 0.65 and for SWE being r = 0.8.

These results could not be reproduced when investigating the relationship between ΔHS/ΔSWE and HS/SWE. Plotting ΔHS against aspect for Monbiel data they show a minor correlation, which cannot be statistically proven though. For the other combinations no correlation is visible. Likewise there was no continuous correlation trend between ΔHS/ΔSWE or HS/SWE and elevation seen. Only for initial HS at Sertig a correlation was found.

7. Discussion

7.1 Applying hysteresis approach to GPR data

Previous research has shown that during snow ablation mean HS constantly decreases while SD of HS stays at a constant level until it drops rapidly due to partial disappearance of snow cover (Egli and Jonas 2009; Egli et al. 2012). As shown in Figure 30 a similar trend is visible in our data. In Monbiel SD even increases for a bit, while Sertig stays at the same level. The relationship between mean SWE and SD of SWE has not yet been investigated. The GPR-data shows thus, apart from an out layer in the Sertig data set a very similar relationship. Also when comparing total C_v and of time steps values for HS and SWE (Table 6 and 7) some similarities are shown. C_v of SWE tends to yield slightly higher values. Looking at Figure 31 basically confirms the effect shown with the different time steps of Figure 30: Monbiel shows increasing variability of the snow cover with time, whereas in Sertig rather similar / random HS/SWE variability can be observed.

Table 9. Crossreference of GPR-data HS mean to HS SD relationship to previously shown ones (Egli and Jonas 2009; Egli et al. 2012).

Data	Scale	Ratio (SD HS : Mean HS)
GPR-data 2015: Monbiel	20m	1:8 (SWE: 1:4)
GPR-data 2015: Sertig	20m	1:6 (SWE: 1:4)
Wannengrat (Egli et al. 2012)	500m	1:6
Imisstations (Egli and Jonas 2009)	20km	1:3

If Figure 19, the variogram of Schirmer & Lehning (2011) is stretched in order to fit the higher scales of previous research, it shows that the outcome of observed ratio (SD HS : Mean HS) is comparable to Egli and Jonas (2009) and Egli et al. (2012). While SWE follows similar trend when looking at C_v the ratio of SD SE to Mean SWE proved to be much smaller. It could be interpreted that a substantial part of ΔHS is only due to a loss of height than actual melt. If this difference of ratios between HS and SWE could be reproduced in other terrain, it would emphasize the use of measures / models that also take in account SWE and not rely on changes in HS only.

Interesting to see when looking at Table 6 and Table 7 is also the increase of C_v at Monbiel for both HS and even more for SWE. At the fieldsite of Sertig, however, this trend cannot be seen as clearly. This implies that during melt season the variability in snow cover can increase. This was not noticed as such by Egli & Jonas (2009) / Egli et al. (2012). A similar trend was observed by Winstral and

Marks (2014). They found increasing C_v when comparing 10 years of measurements from January and April of a catchment in southwest Idaho, USA. Changes in C_v develop when either there is a greater variability in snow accumulations present or only a decrease of HS, not snow melt itself is measured (Winstral and Marks 2014). When looking at Table 6 it can be shown that HS variability (see SD HS) increases slightly for Monbiel, but stays roughly at the same level. Although when looking at SWE the increasing trend of SD SWE at Monbiel is somewhat bigger. All in all the measurements confirm actual snowmelt. There are some exceptions (e.g. M6 and M7), where there is a different relative decrease between HS and SWE (see Figure 34, Figure 35). A further explanation for varying C_v could be an anti-correlation between accumulation and snow melt rates. To find out if this could be the case, it would be necessary to observe both accumulation patterns as well as snow ablation patterns in a next field campaign. Whatever the reason is for an increasing C_v in Monbiel it would be interesting to further investigate that matter. It would be especially interesting to conduct further research in different valleys in order to get significant results concerning homogenous or heterogeneous melt rates.

7.2 Terrain Roughness and Snow Cover

Diverse analysis methods were chosen to investigate whether and to what extent terrain roughness influences snow cover (changes).

Based on the fact that rough terrain yields a higher variation of HS/SWE distribution with rough terrain, it was investigated whether C_v of HS/SWE and modelled terrain roughness correlate (see Figure 31). The results showed a weak correlation between the two variables. It is though important to note that the ratio between rough and smooth data is very uneven and thus the results may not be representative. Nevertheless, it is interesting to see that apparently there is a close to linear relationship between increasing HS/SWE variability with terrain. The roughness measure, even if averaged seems to provide realistic results. If this relationship could be proved for other data this could be very interesting to be able to predict HS/SWE variability with the local roughness level.

Comparing roughness to initial HS / SWE or ΔHS / ΔSWE did not show any correlation. This does not come as a surprise, since snow has the effect of smoothening out terrain roughness. To estimate winter roughness from summer roughness Veitinger (2015) found out that using a bigger window size for VRM does imitate winter roughness to a certain point. Depending on HS a different window for VRM analysis needs to be chosen (VRM). Applying this observation to the measured GPR-data though did not show a better correlation between "modelled winter terrain roughness " and initial HS / SWE or ΔHS / ΔSWE. To really estimate winter surface for Monbiel and Sertig repeated LiDAR scan or a similar method would be necessary.

Even if no direct correlation has been found between terrain roughness and initial HS / SWE or ΔHS / ΔSWE following points should be mentioned: In the first place, C_v proved to be conceptually and at least visually, even if not entirely statistically, correlated with terrain roughness. Conversely terrain roughness could be taken as an indicator for a snow cover that yields more HS and SWE variability in rough terrain than in smooth terrain (wind factored out). Moreover, it was visually noticed during the measurement campaigns that rough terrain tends much more to show patchy melt out patterns. For example Figure 28 taken on the last campaign of Sertig shows nicely how the rougher terrain already shows snow free patches, while the flat area before still looks very homogenous and smooth. Despite not measuring those observation it can be held on to the fact that rough terrain is "more special" and needs more attention than flat one.

To be able to make a difference between rough and smooth terrain a suitable roughness measure is needed. VRM / CVRM were found to be a very convincing way to represent roughness. On the one hand VRM / CVRM are based on a terrain model and can be calculated without any effort. This stands as opposite to Lehning et al. (2011), who used fractals to assess terrain roughness. Fractals are without any doubt a very sophisticated way to model terrain roughness, especially since it can adapt to different spatial scales (Lehning et al. 2011). However, fractals are calculated along lines and are computationally intensive (Helbig et al. 2015). Nevertheless, the roughness measures VRM and CVRM proofed to model terrain very correctly without correlating to slope. Being of the opinion that VRM and CVRM are very suitable roughness approaches it would be interesting to see whether it could be used to assess snow accumulation in a similar way than done by Helbig et al. (2015), Lehning et al. (2011) or Revuelto et al. (2014).

7.4 Heterogeneous snow melt

A hint that heterogeneous snowmelt occurs in the investigated fieldsites is given by **Fehler! Verweisquelle konnte nicht gefunden werden.**, where melt rates of two different time steps were plotted against each other. It was observed that transect itself showed very homogenous melt, while between transects differences existed. Such differences were more distinct at Monbiel. At Sertig transects are also slightly lumped, show especially for SWE a rather random pattern. For the difference between ΔHS1 and ΔHS2 it can be assumed that during first measurements snow cover was still settling after the snowfall in the end of March. For ΔHS2 this process seemed to play a smaller role. Having discovered heterogeneous melt rates at Monbiel might bring the increasing C_v rates of both HS and SWE in a different light. Optionally, increasing C_v may be interpreted as a sign for heterogeneous melt at Monbiel. However to postulate such an idea much more data and fieldsites would be needed.

Of course, the question of how these differences can be explained was soon to be raised. Looking at the correlation between ΔHS / ΔSWE and aspect, only a slight correlation could be observed for the pair Monbiel / ΔHS. However, at Monbiel a correlation between ΔH / ΔSWE and slope was observed, which is opposed by a slight anti-correlation when slope and HS /SWE at POW are compared. For Sertig only a positive correlation between HS /SWE at POW and slope was found. For Monbiel this means that less snow is accumulated at steeper parts, but flatter parts less melt than steeper parts.

In summary, Monbiel shows distinct heterogeneous snowmelt and a positive correlation between ΔH / ΔSWE and slope.However, Sertig does not have such clear trends. It is therefore asked what the underlying reason for this difference is. If one compares the two fieldsites, two essential differences meet the eye. Firstly, the transects at Monbiel are mostly southerly exposed, whereas the transects at Sertig yield a mostly southerly exposition. Furthermore, the measurements at Sertig were taken one month later than at Monbiel. Before starting making hypotheses it should not be forgotten that the data amount, transect lengths and number, elevation and many more other differences exist between the catchment and it is thus not possible to find the ultimate solution. Combining those two observations it stands to reason that differences in radiation and solar angle could play a role. As Anderton et al. 2004 noted are terrain characteristics more important in early melt season than later onwards. To illustrate this reasoning using ArcGIS a global radiation map for the measurement period of Monbiel, as well as the measurement period of Sertig was calculated, see Figure 38. To model global radiation ArcGIS combines direct radiation and diffuse radiation for the specified time period. For this ArcGIS uses method by Fu and Rich (2002) that are based on the given topography, the solar angle corresponding to modelling time window and the solar constant. It is therefore a simple approach, but it shows clearly the tendencies that could cause the difference in melting patterns between Monbiel and Sertig. It has to mentioned that the scales are not normalized, nevertheless it is observable that the fieldsites at Monbiel experience different amount of solar radiation, whereas at Sertig all transects receive approximately the same amount. To quantify these differences as well as evaluate, which radiation / fluxes are real essential more research would have to be done. For example it could be possible to model the components of the energy balance for the transects by using a sophisticated physical model (Lehning et al. 2006). In such a case it is important not only to include global radiation but also other heat fluxes (Helbig et al. 2010).

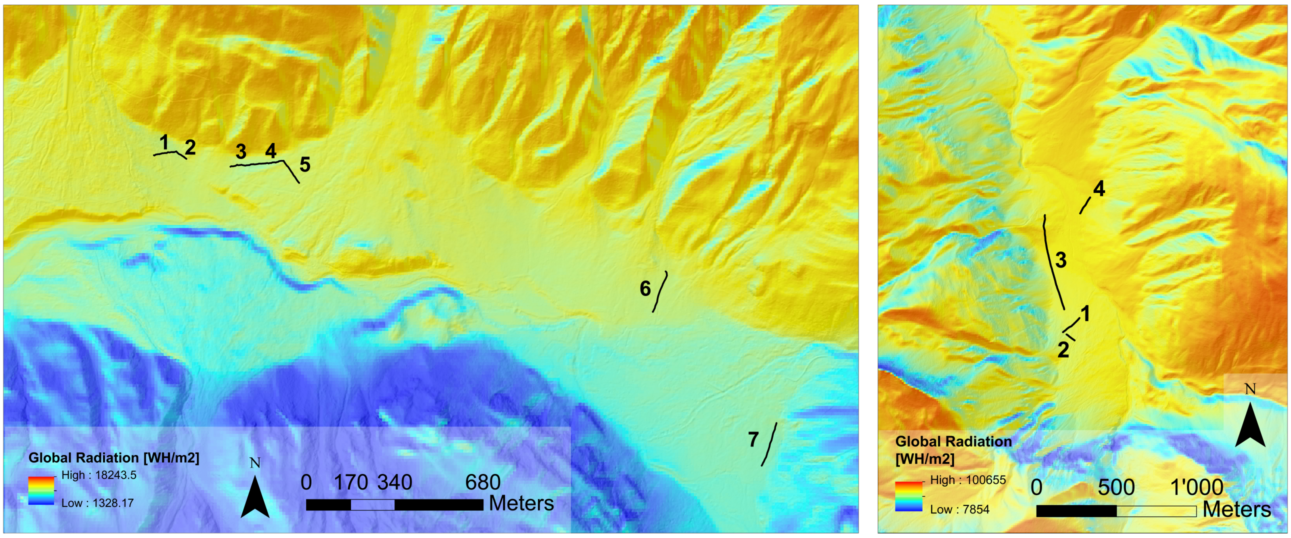

Figure 37. Global radiation for the correspondent measurement ranges. Range of global radiation is not normalized, there are therefore a corresponding maxima / minima for both Monbiel and Sertig.

7 Conclusion and Outlook

Out of the multiple analyses following conclusions could be drawn:

It was found that it is possible to measure SWE and HS with a GPR in a satisfying way that yields a similar accuracy to other measurement systems like LiDAR. In order to make differential measurements it is essential that HS1/SWE1 and HS2/SWE2 differ enough to be higher than the RMSE. This was here only partly given. Due to measurement path differences of the different dates and due to scattered HS/SWE output makes sense to calculate ΔHS/ΔSWE with mean values in order to not let outliers influence the result. As absolute measurements HS as well as SWE work well.

The hysteresis effect discovered by Egli and Jonas (2009) and was reinforced by Egli et al. (2012) does also apply in general to the measured HS data: Mean HS rapidly decreases and SD HS stays similar or even increases. Also it was found that SWE behaves similarly. SWE does yield a differentiation between mean HS and SD HS though. Why Cv at Monbiel rises could not be found out. Explanation range from increasing SD, to random finding to a possible sign that heterogeneous snowmelt was prevailing at Monbiel.

Despite not being able to find a direct correlation between either HS/SWE or ΔHS/ΔSWE it was found that terrain roughness plays an important part for snow cover. The chosen roughness measure showed a slight correlation to C_v. If this finding could be confirmed by different data it would be interesting to find out whether terrain roughness could be used to predict C_v. Therefore terrain roughness is more important for snow cover build up. As many studies have shown initial snow cover is very relevant for snowmelt patterns. It can therefore be said that indirectly terrain roughness has an effect on snow melt by providing different snow cover architecture than in smooth terrain.

At the fieldsite of Monbiel heterogeneous melt was found, whereas in Sertig not such a clear determination was possible. Statistical correlation for heterogeneous melt was only found when looking at ΔHS/ΔSWE and slope at Monbiel. Based on the assumption that solar angle could play a role, a solar radiation map was calculated using ArcGIS. In Monbiel daily solar radiation for the different transects differed a lot during measurement period, whereas during measurements at Sertig the sun already had a higher angle and brought more uniform radiation down to the valley. To quantify such a relationship, solar radiation as well as heat fluxes would have to be measured or modelled by applying a physical snow cover model.

All in all it can be said that both homogenous and heterogeneous melt approach have their validity. The heterogeneous melt approach especially is valid early in season. Later in season a homogenous approach applies just as well in similar slopes. This might not be valley for the comparison of steep north slopes and steep south slopes. It would be interesting to find out how a model would perform that applies heterogeneous melt in early winter until a certain solar angle is reached and then would proceed using homogenous melt rates.

Literature

Anderton, S. P., White S. M., and Alvera B. 2002. “Micro-Scale Spatial Variability and the Timing of Snow Melt Runoff in a High Mountain Catchment.” *Journal of Hydrology* 268:158–176.

Anderton, S. P., White S.M., and Alvera B. 2004. “Evaluation of Spatial Variability in Snow Water Equivalent for a High Mountain Catchment.” *Hydrological Processes* 18(3):435–453.

Annan, A. P. 2009. “Electromagnetical Principles of Ground Penetrating Radar.” P. 524 in *Ground Penetrating Radar: Theory and Applications.*, edited by Jol, H. M.. Amsterdam: Elsevier Science & Technology.

Bradford, J. H., Harper J.T., and Brown J. 2009. “Complex Dielectric Permittivity Measurements from Ground-Penetrating Radar Data to Estimate Snow Liquid Water Content in the Pendular Regime.” *Water Resources Research* 45(8):1–12.

Brubaker, K. M et al. 2013. “The Use of LiDAR Terrain Data in Characterizing Surface Roughness and Microtopography.” *Applied and Environmental Soil Sciences*, 1–13.

Bühler, Y. et al. 2015. “Snow Depth Mapping in High-Alpine Catchments Using Digital Photogrammetry.” *The Cryosphere* 9(1):229–243.

Burrough, P. A. and McDonnell R. A. 1998. *Principles of Geographical Information Systems*. Oxford University Press.

Corripio, J. G. 2003. “Vectorial Algebra Algorithms for Calculating Terrain Parameters from DEMs and Solar Radiation Modelling in Mountainous Terrain.” *International Journal of Geographical Information Science* 17(1):1–23.

Debeer, Ch. M. and Pomeroy, J. W. 2009. “Modelling Snow Melt and Snowcover Depletion in a Small Alpine Cirque , Canadian Rocky Mountains.” *Hydrological Processes* 23:2584–2599.

Egli, L. and Jonas, T. 2009. “Hysteretic Dynamics of Seasonal Snow Depth Distribution in the Swiss Alps.” *Geophysical Research Letters* 36(2).

Egli, L. 2011. “Spatial Variability of Seasonal Snow Cover at Different Scales in the Swiss Alps.” 52(58):9–14.

Egli, L., Jonas T., Grünewald, T., Schirmer, M., and Burlando, P. 2012. “Dynamics of Snow Ablation in a Small Alpine Catchment Observed by Repeated Terrestrial Laser Scans.” *Hydrological Processes* 26(10):1574–1585.

Fu, P. and Rich, P. M. 2002. “A Geometric Solar Radiation Model with Applications in Agriculture and Forestry.” 37.

Grenfell, T. C. and Putkonen, J. 2008. “A Method for the Detection of the Severe Rain-on-Snow Event on Banks Island, October 2003, Using Passive Microwave Remote Sensing.” *Water Resources Research* 44(3).

Grohmann, C. H., Smith, M. J., and Riccomini C. 2011. “Multiscale Analysis of Topographic Surface Roughness in the Midland Valley , Scotland.” *IEEE Transactions on Geoscience and Remote Sensing* 49(4):1200–1213.

Grünewald, T. et al. 2013. “Statistical Modelling of the Snow Depth Distribution in Open Alpine Terrain.” *Hydrology and Earth System Sciences* 17(8):3005–3021.

Gustafsson, D., Sundström N., and Lundberg A. 2012. “Estimation of Snow Water Equivalent of Dry Snowpacks Using a Multi-Offset Ground Penetrating Radar System.” Pp. 197–206 in *69th Eastern Snow Converence, Frost Valley YMCY, Claryville, New York, USA 2012*.

Helbig, N., Van Herwijnen, A., Magnusson J., and Jonas, T. 2014. “Fractional Snow-Covered Area Parameterization over Complex Topography.” *Hydrology and Earth System Sciences Discussions* 11(8):9791–9827.

Helbig, N., Van Herwijnen, A., Magnusson J., and Jonas, T. 2015. “Fractional Snow-Covered Area Parameterization over Complex Topography.” *Hydrology and Earth System Sciences* 19(3):1339–1351.

Helbig, N., Löwe, H., Mayer, B., and Lehning, M.. 2010. “Explicit Validation of a Surface Shortwave Radiation Balance Model over Snow-Covered Complex Terrain.” *Journal of Geophysical Research* 115:1–12.

Hengl, T. 2006. “Finding the Right Pixel Size.” *Computers & Geosciences* 32(9):1283–1298.

Hodgson, M. E. 1995. “The Does Size What Gell Reptesent ? Angle Slope Gomputed / Aspect.” *Photogrammetric Engineering & Remote Sensing* 61(5):513–517.

Jonas, T., Marty, C., and Magnusson J. 2009. “Estimating the Snow Water Equivalent from Snow Depth Measurements in the Swiss Alps.” *Journal of Hydrology* 378(1-2):161–167.

Lehning, M. et al. 2006. “ALPINE3D : A Detailed Model of Mountain Surface Processes and Its Application to Snow Hydrology.” *Hydrological Processes* 20(10): 2111–2128.

Lehning, M., Grünewald, T., and Schirmer, M. 2011. “Mountain Snow Distribution Governed by an Altitudinal Gradient and Terrain Roughness.” *Geophysical Research Letters* 38:1–5.

Looyenga, H. 1965. “Dielectric Constants of Heterogenous Mixtures.” *Physica* 31:401–406.

Lundberg, A., Richardson-Näslund, C., and Andersson C. 2006. “Snow Density Variations: Consequences for Ground-Penetrating Radar.” *Hydrological Processes* 20:1483–1495.

Melvold, K. and Skaugen T. 2013. “Multiscale Spatial Variability of Lidar-Derived and Modeled Snow Depth on Hardangervidda, Norway.” *Annals of Glaciology* 54(62):273–281.

Olaya, V. 2009. “Basic Land-Surface Parameters.” Pp. 141–69 in *Geomorphometry: Concepts, Software, Applications*, vol. 33, edited by Reuter, H. and Hengl, T. Elsevier.

Pohl, S. et al. 2006. “Spatial-Temporal Variability in Turbulent Fluxes during Spring Snowmelt Spatial-Temporal Variability in Turbulent Fluxes during Spring Snowmelt.” 38(1):136–146.

Pomeroy, J. W., Toth, B., Granger, R. J., and Essery, R. L. H. 2003. “Variation in Surface Energetics during Snowmelt in a Subarctic Mountain Catchment.” *Journal of Hydrometeorology* 4:702–719.

Revuelto, J., López-Moreno, J. I., Azorin-Molina, C., and Vicente-Serrano, S.M. 2014. “Topographic Control of Snowpack Distribution in a Small Catchment in the Central Spanish Pyrenees: Intra- and Inter-Annual Persistence.” *The Cryosphere* 8(5): 1989–2006.

Sappington, J. M., Longshore, K. M., and Thompson, D. B. 2007. “Quantifying Landscape Ruggedness for Animal Habitat Analysis: A Case Study Using Bighorn Sheep in the Mojave Desert.” *Journal of Wildlife Management* 71(5):1419–1426.

Schirmer, M. and Lehning, M. 2011. “Persistence in Intra-Annual Snow Depth Distribution: 2. Fractal Analysis of Snow Depth Development.” *Water Resources Research* 47(9).

Sundström, N., Kruglyak, A., and Friborg, J. 2012. “Modeling and Simulation of GPR Wave Propagation through Wet Snowpacks: Testing the Sensitivity of a Method for Snow Water Equivalent Estimation.” *Cold Regions Science and Technology* 74-75:11–20.

Takahashi, K., Igel, J., Preetz, H., and Kuroda, S. 2012. “Basics and Application of Ground- Penetrating Radar as a Tool for Monitoring Irrigation Process.” Chapter 8 in Problems, *Perspectives and Challenges of Agricultural Water Management*., edited by Kumar, M. Intech.

Trujillo, E., Ram, J. A., and Elder, K. J. 2009. “Scaling Properties and Spatial Organization of Snow Depth Fields in Sub-Alpine Forest and Alpine Tundra.” *Hydrological Processes* 23(11).

Veitinger, J., Sovilla B., and Purves, R. S. 2014. “Influence of Snow Depth Distribution on Surface Roughness in Alpine Terrain: A Multi-Scale Approach.” *The Cryosphere* 8(2):547–569.

Veitinger, J. 2015. “Release Areas of Snow Avalanches : New Methods and Parameters.” University of Zurich.

Winstral, A. and Marks, D. 2014. “Long-Term Snow Distribution Observations in a Mountain Catchment: Assessing Variability, Time Stability, and the Representativeness of an Index Site.” *Water Resources Research* 50:293–305.

Winstral, A., Marks, D., and Gurney, R. 2009. “An Efficient Method for Distributing Wind Speeds over Heterogeneous Terrain.” *Hydrological Processes* 23(17):2526–2535.

Appendix

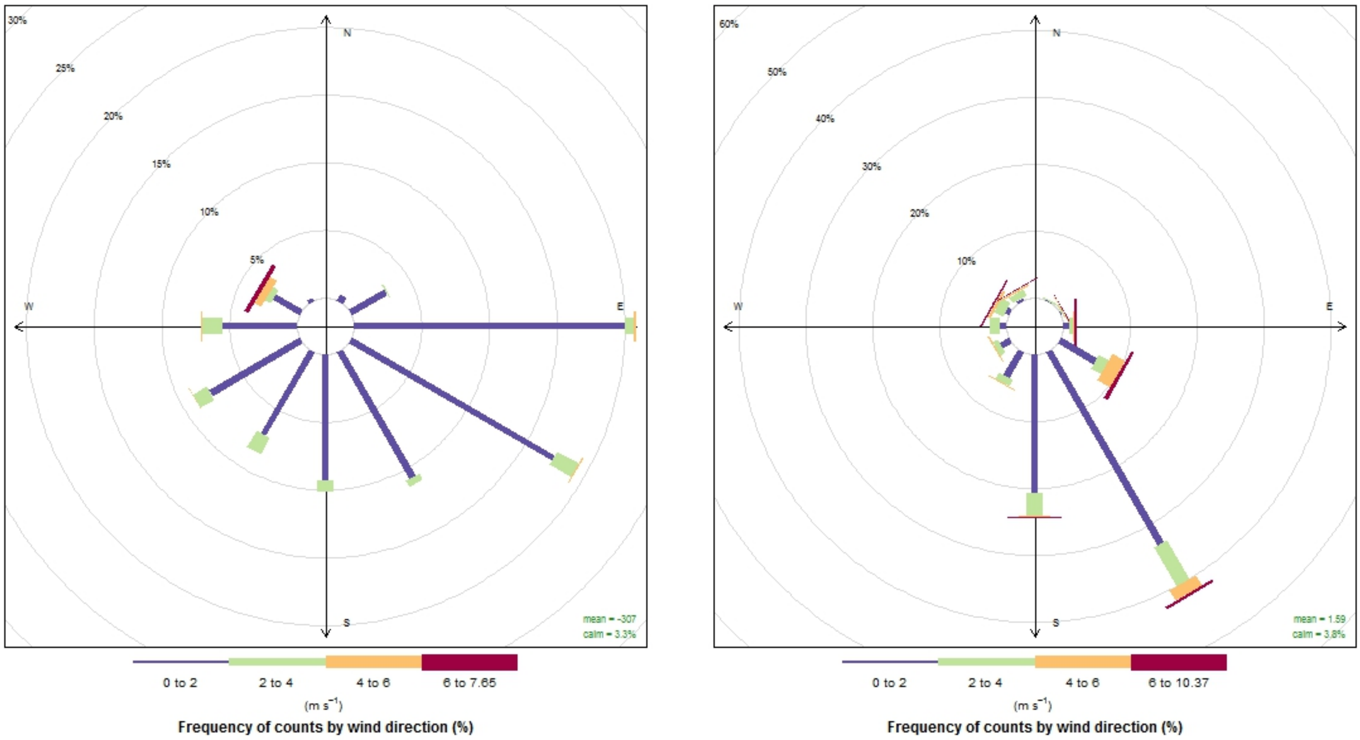

Figure 38. Wind direction and velocity at meteo station Pardenner Boden (left) and Sertig (right).

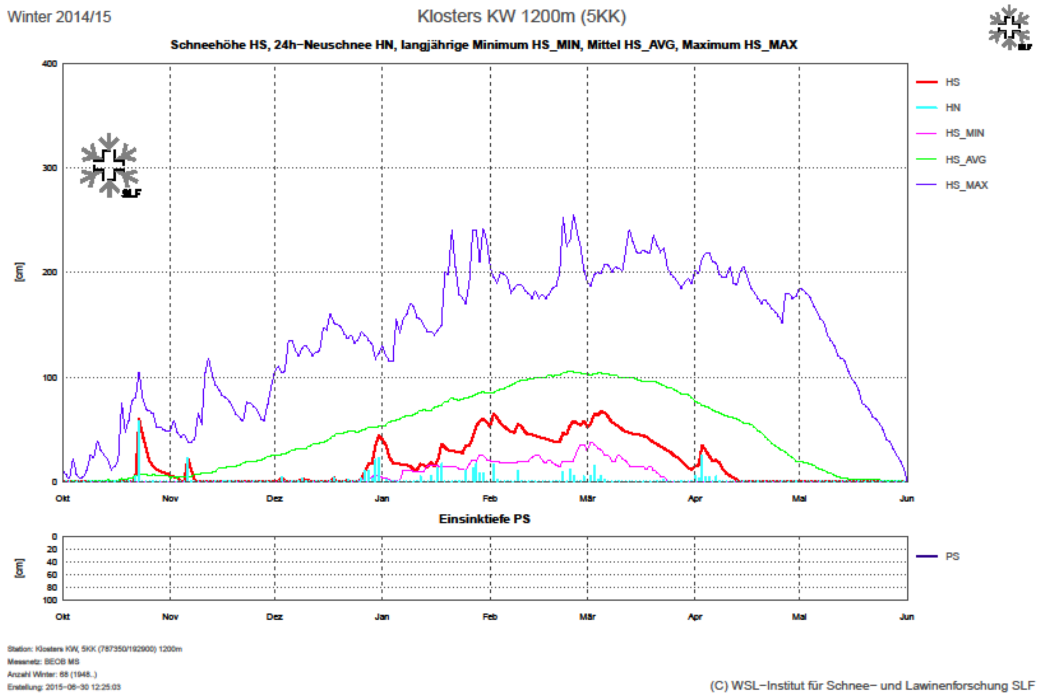

Figure 39. Observer data from Klosters KW (1200m a.s.l., 787350/192900).

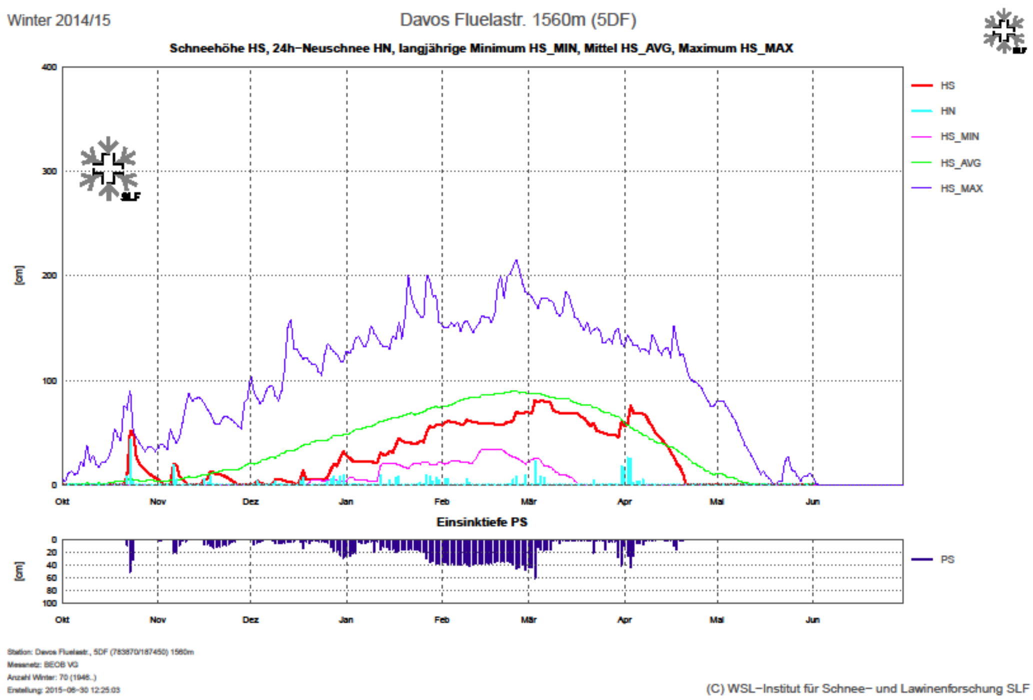

Figure 40. Observer data from Davos Fluelastrasse (1560m a.s.l., 783870/187450).

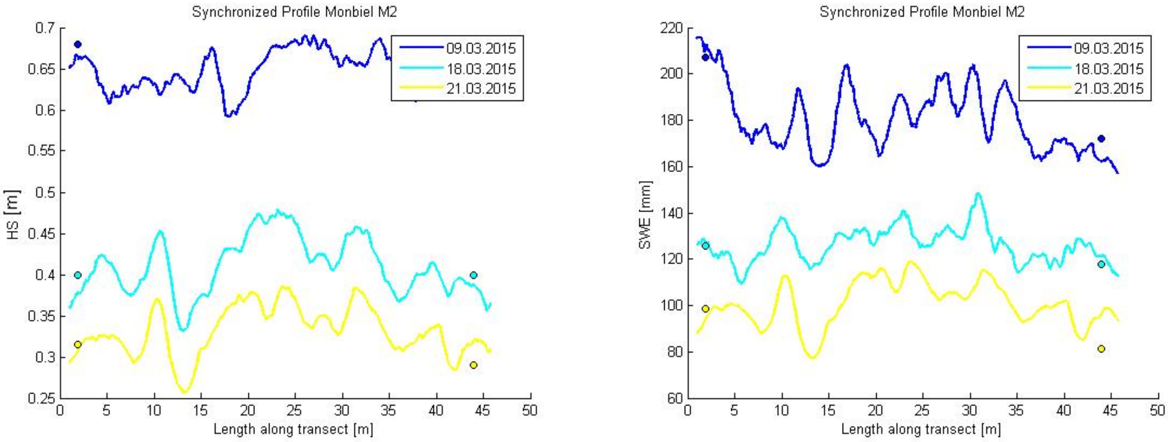

Figure 41. Measured HS and SWE values from transect M2 at different timesteps.

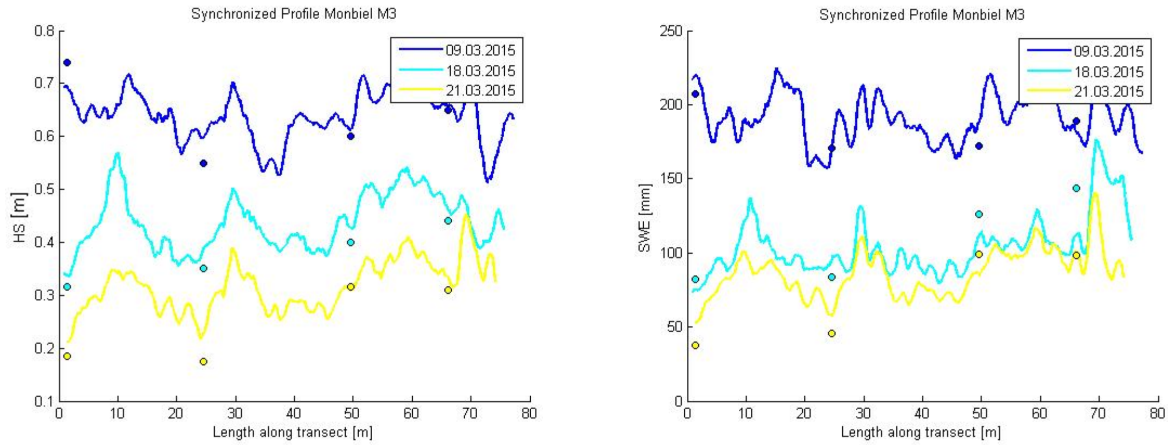

Figure 42. Measured HS and SWE values from transect M3 at different timesteps.

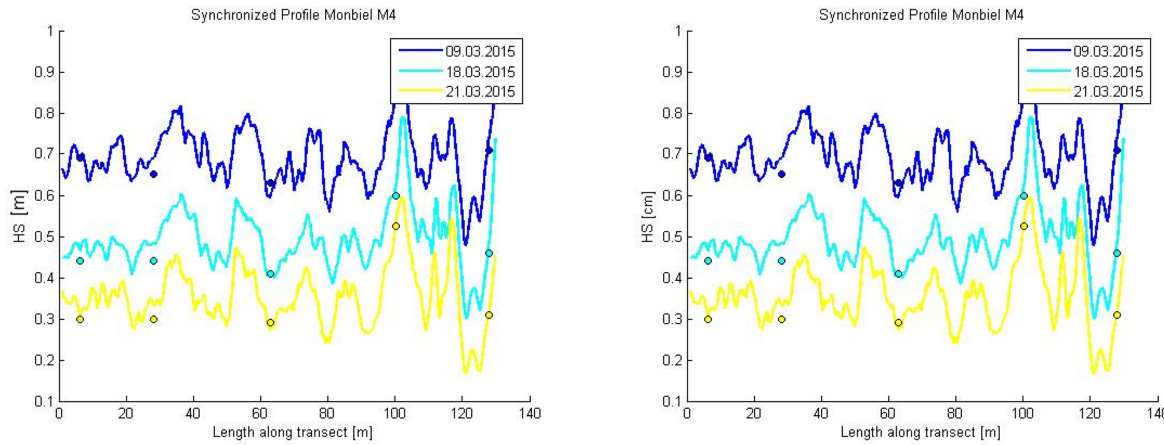

Figure 43. Measured HS and SWE values from transect M4 at different timesteps.

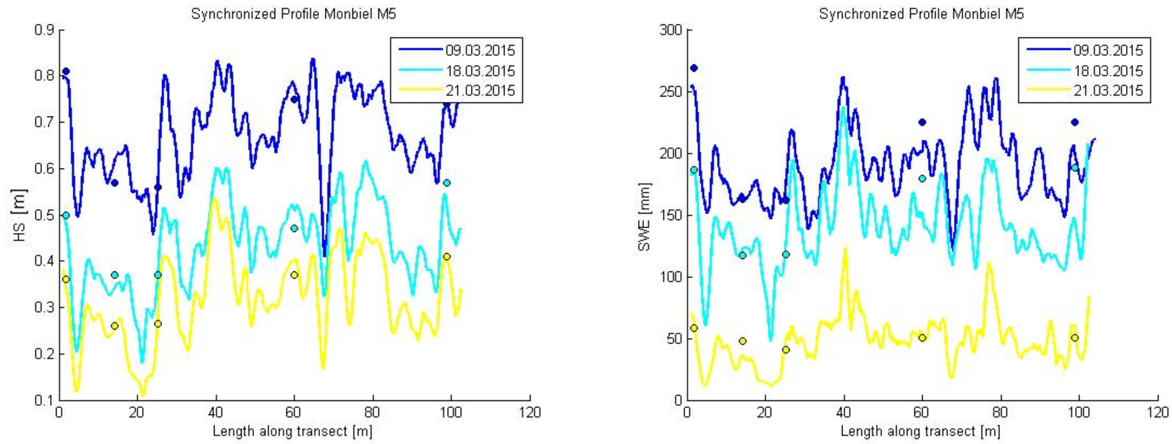

Figure 44. Measured HS and SWE values from transect M5 at different timesteps.

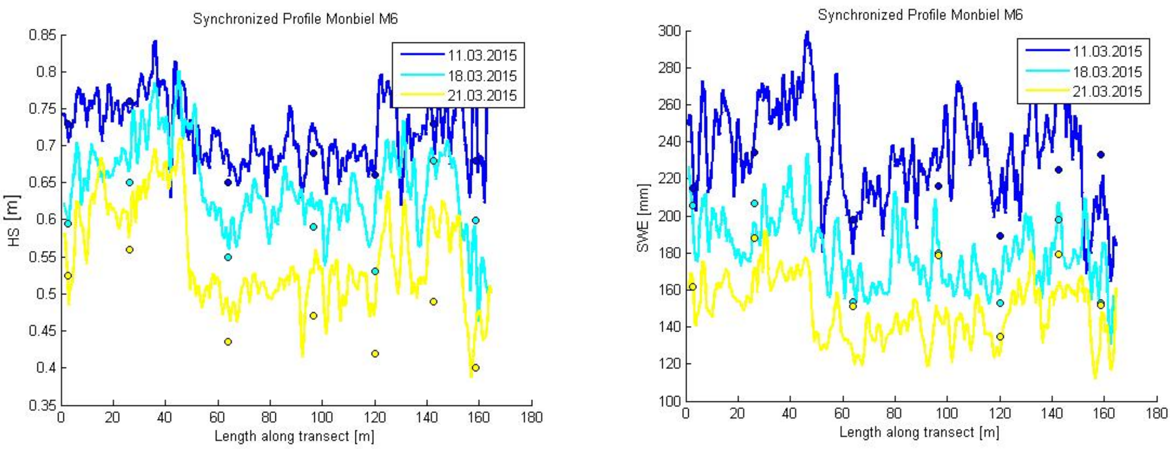

Figure 45. Measured HS and SWE values from transect M6 at different timesteps.

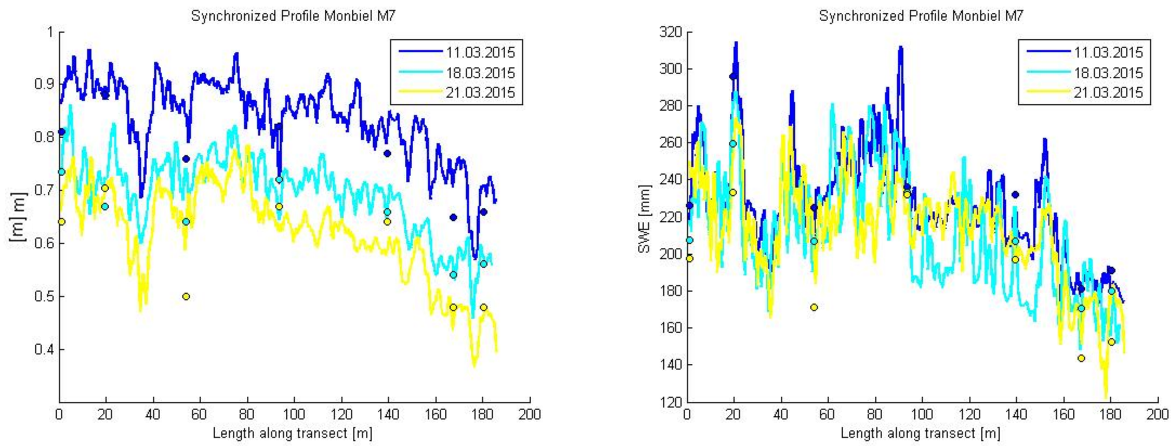

Figure 46. Measured HS and SWE values from transect M7 at different timesteps.

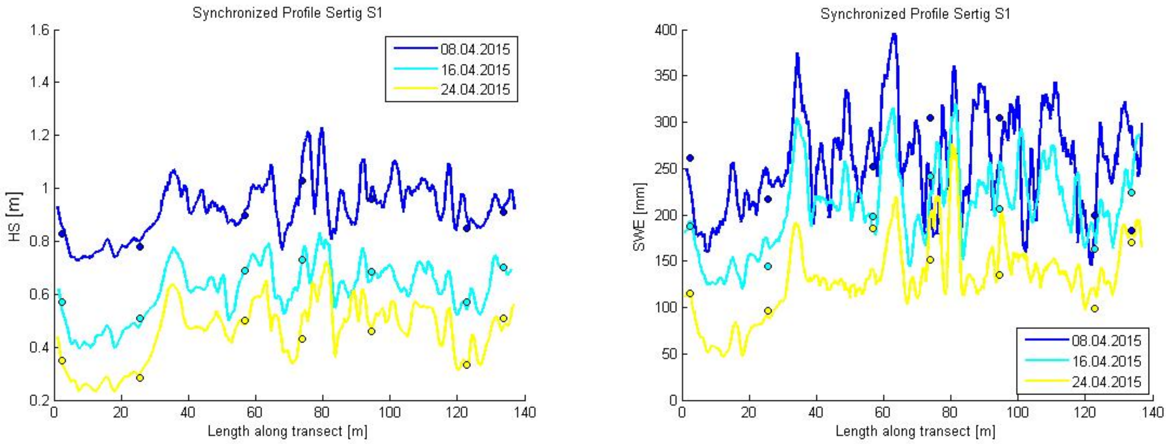

Figure 47. Measured HS and SWE values from transect S1 at different timesteps.

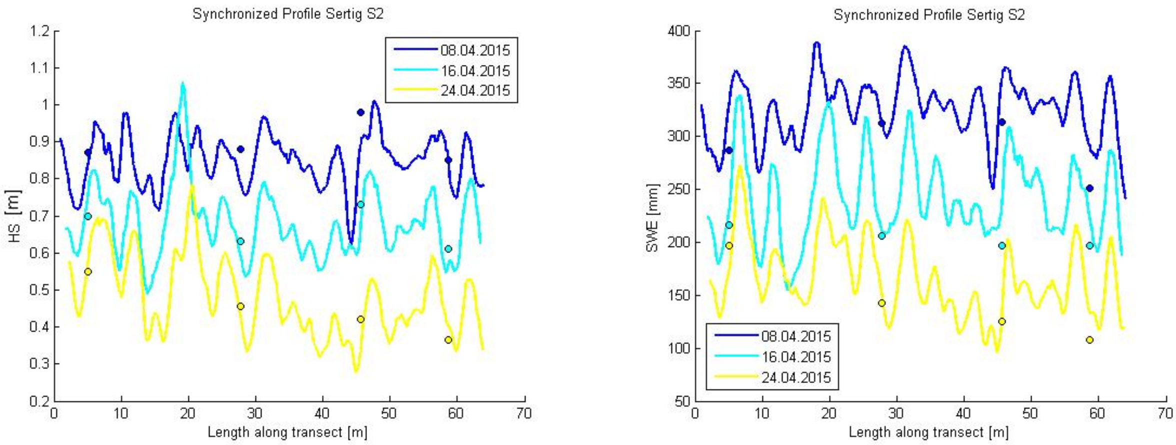

Figure 48. Measured HS and SWE values from transect S2 at different timesteps.

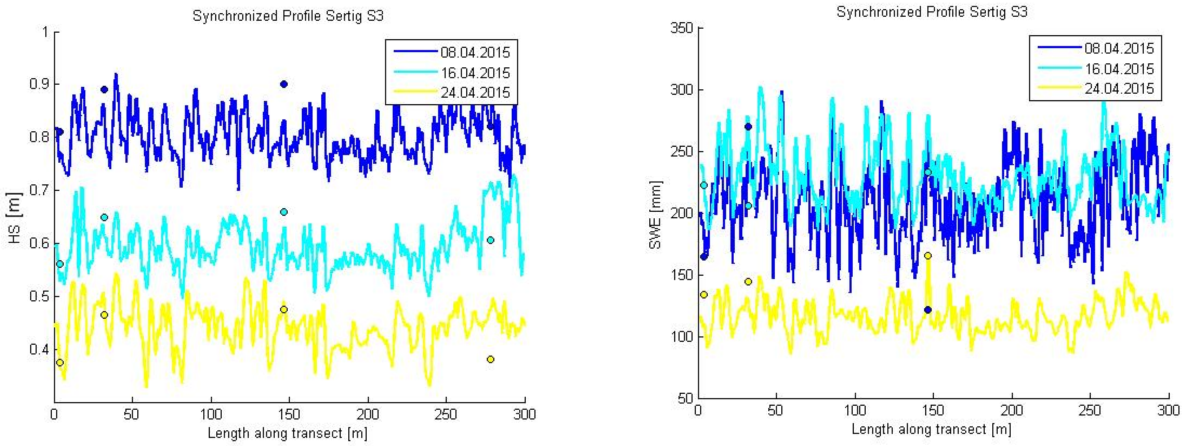

Figure 49. Measured HS and SWE values from transect S3 at different timesteps.

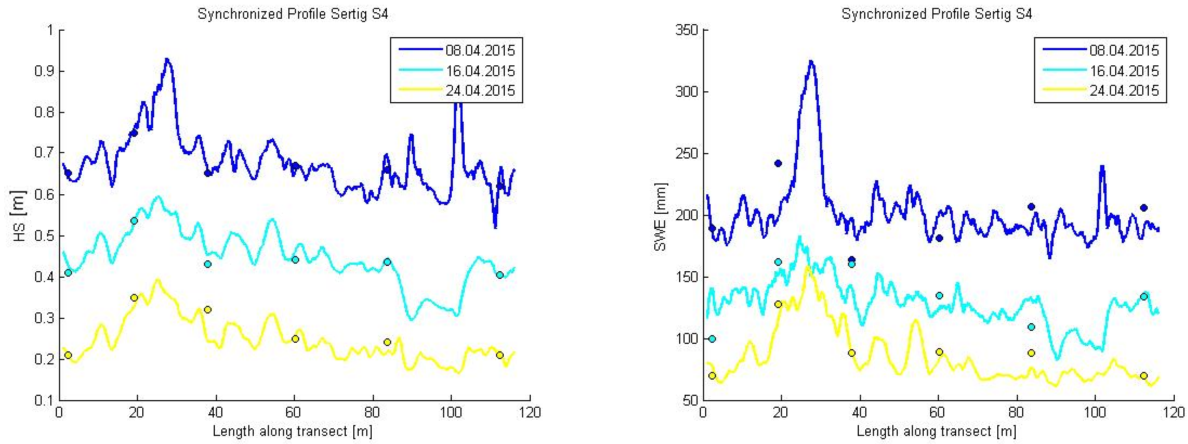

Figure 50. Measured HS and SWE values from transect S4 at different timesteps.

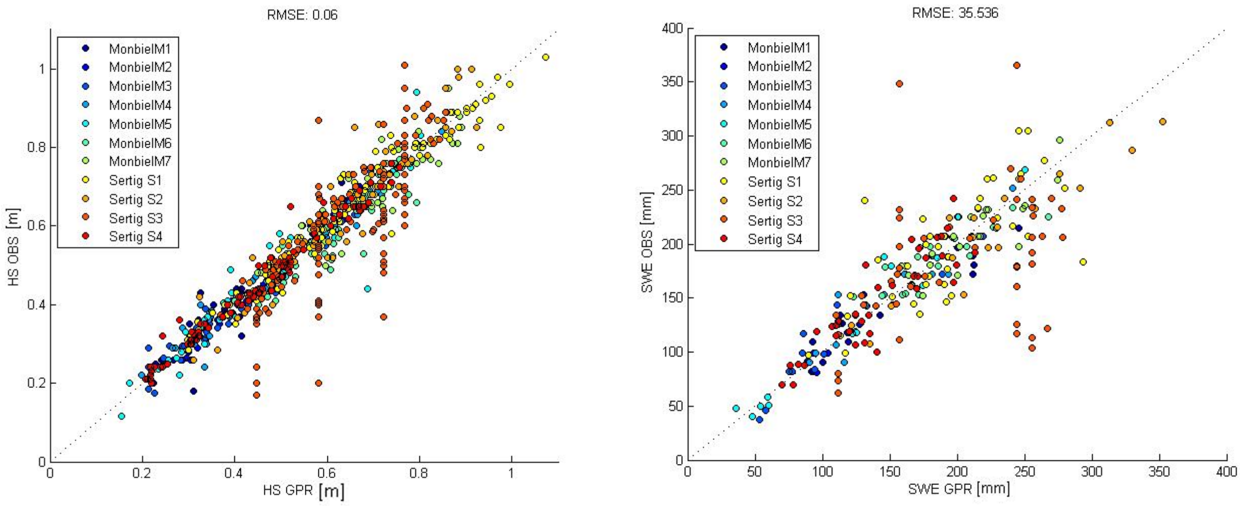

Figure 51. RMSE of manual measurements against GPR measurements, taking into account all the transects

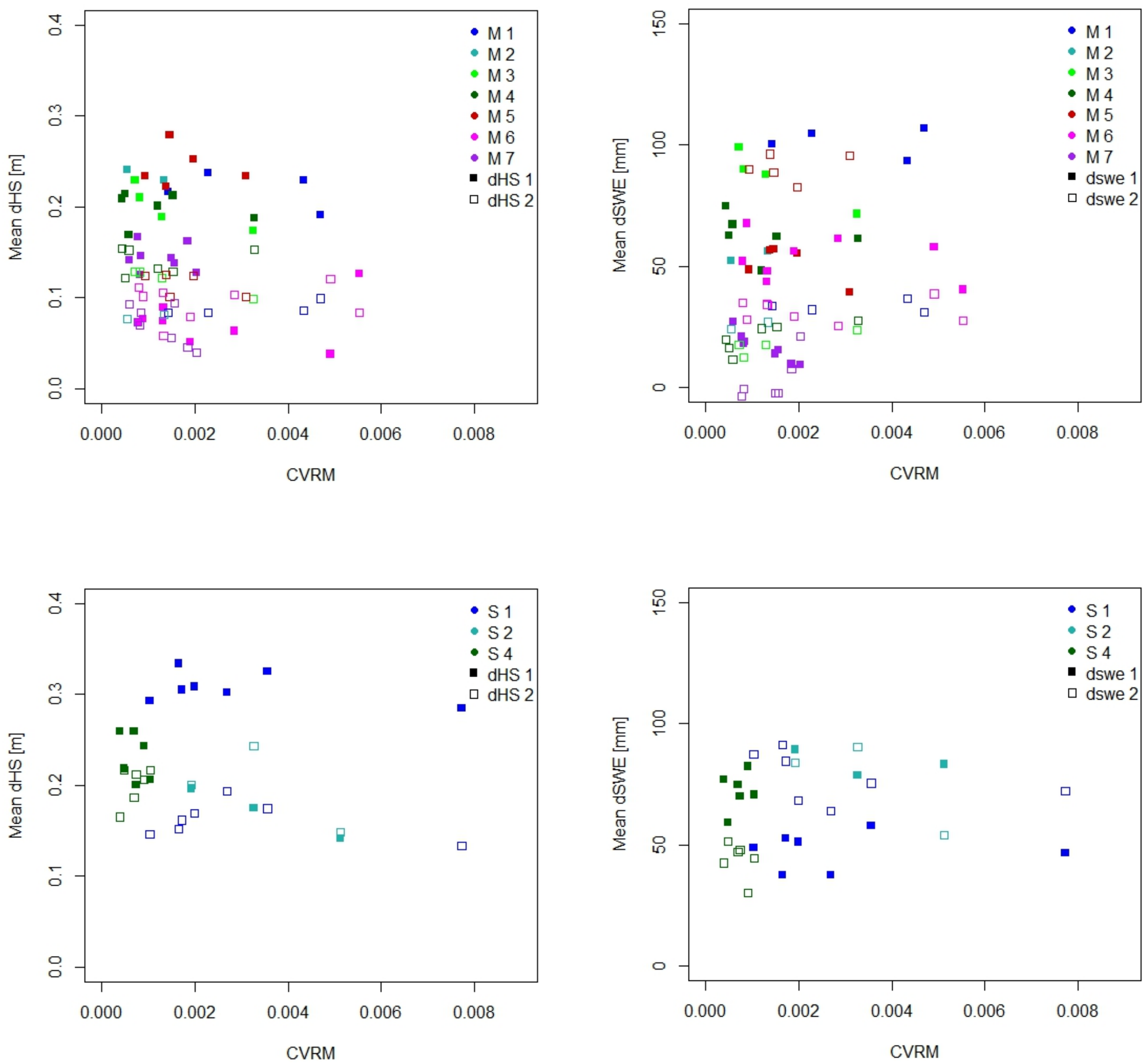

Figure 52. ΔHS1/ΔSWE1 and ΔHS2/ΔSWE2 plotted against CVRM.

R code CVRM

```
rm(list = ls())
setwd("/D:/r_stuff/")

## Prep
library(SDMTools)
library(R.methodsS3)
library(R.oo)
library(R.utils)
library(ascii)
library(insol)
library(raster)
###############################################################################################
###############
## Get data
dem <- as.matrix(read.table("D:/r_stuff/data/dtm/tlm12.asc", skip=6, na.strings="-9999"))
dem_head <- read.table("D:/r_stuff/data/dtm/tlm12.asc", nrow=6)

cellsize <- 2
header    <-    rbind(paste("ncols",dem_head[1,2],sep="    "),paste("nrows",dem_head[2,2],sep="
"),paste("xllcorner",dem_head[3,2],sep=" "),paste("yllcorner",dem_head[4,2],sep=" "),
                paste("cellsize",dem_head[5,2],sep="
"),paste("NODATA_value",dem_head[6,2],sep=" "))

###############################################################################################
################
# ## calculates components of vector for each cell

dlx = 2
dly = 2

row = nrow(dem)
col = ncol(dem)

# dem = as.matrix(dem)
md = dem [-row, -1]
mr = dem [-1, -col]
mrd = dem [-1, -1]

y_matrix = 0.5 * dlx * (dem[-row, -col] + md - mr - mrd)
x_matrix = 0.5 * dly * (dem[-row, -col] - md + mr - mrd)
z_matrix = matrix((dlx * dly), nrow=nrow(x_matrix), ncol=ncol(x_matrix))

y_matrix <- cbind(y_matrix, y_matrix[,ncol(y_matrix)])
y_matrix <- rbind(y_matrix, y_matrix[nrow(y_matrix),])

x_matrix <- cbind(x_matrix, x_matrix[,ncol(x_matrix)])
x_matrix <- rbind(x_matrix, x_matrix[nrow(x_matrix),])
```

```
z_matrix <- cbind(z_matrix, z_matrix[,ncol(z_matrix)])
z_matrix <- rbind(z_matrix, z_matrix[nrow(z_matrix),])

####create unit vector / components
##############################################################################################
#################
## calculate roughness with vectors calculate above joanna style#

x_raster <- raster(x_vector)
x_raster <- focal(x_raster, w=matrix(1,3,3), fun = sum) #uses raster packages

y_raster <- raster(y_vector)
y_raster <- focal(y_raster, w=matrix(1,3,3), fun = sum)

z_raster <- raster(z_vector)
z_raster <- focal(z_raster, w=matrix(1,3,3), fun = sum)


result_raster <- sqrt((x_raster)^2 + (y_raster)^2 + (z_raster)^2)

ruggedness_raster<- (1- (result_raster/9))

plot(ruggedness_raster)

##############################################################################################
#######################
######### storing files
ruggedness_raster[is.na(ruggedness_raster)] <- -9999
ruggedness <- as.matrix(ruggedness_raster)
ff = "D:/gis/corripio_tlm12.asc"

cat(header, file = ff, sep = '\n')
write.table(ruggedness, file = ff, append = TRUE, col.names = FALSE, row.names = FALSE, sep =
"\t")
```

Personal Declaration

I hereby declare that the submitted thesis is the result of my own, independent work. All external sources are explicitly acknowledged in the thesis.

Place, Date

Franziska Mohr